UNIVERSITÀ DEGLI STUDI DI PADOVA

DIPARTIMENTO DI INGEGNERIA DELL'INFORMAZIONE

University of Padova Department of Information Engineering

Master Degree in Bioengineering

Pelvic symmetry studied with the segmentation software Materialise for the treatment of acetabulum fractures in Traumatology

Candidate : Stéphane CANDONI

University Supervisor: Prof Emanuele Luigi CARNIEL

Research Supervisor: Martine PITHIOUX, Institut des Sciences du Mouvement

Medical supervisor : Marie LE BARON, Hôpital Nord de Marseille

Academic Year 2023/2024

12 December 2024

INSTITUT DES SCIENCES ETIENNE DU MOUVEMENT JULES MAREY

Centrale Méditerranée

Table of contents

ABSTRACT

This Master Thesis aims to assist orthopedic surgeons in the treatment of pelvic fractures while using osteosynthesis plates. To fabricate pre-operatively patient-specific plates and facilitate the surgical planning process, 3D virtual pelvis models are developed due to the complex structure of the bony pelvis. Modelling helps to understand the characteristics of the fracture and to decrease the duration of surgery and therefore the risk of bleeding. Thus, it improves immediate and longer-term post-operative results.

Currently, these models use the healthy contralateral hemi-pelvis to visualize the fractured hemi-pelvis before the fracture. Consequently, perfect symmetry of the pelvis is assumed. In addition, clinical assessment of surgical treatment is based on criteria such as the Matta scoring system, which also involves symmetry of the pelvis. However, morphological changes related to age and sex can lead to asymmetry of the pelvis. In particular, male and female pelvises evolve differently, due to biological functions such as childbirth for women. Consequently, it is crucial to determine whether or not the pelvis can be considered symmetrical in order to construct the 3D virtual image of the fractured pelvis before the fracture.

In this work, modelling tools are used to compare global and local symmetries of pelvis. Therefore, similarities in regions of interest (defined by the orthopedic surgeon) are analyzed on the basis of CT scan images collected from a cohort of 28 patients with of healthy pelvis. Images are reconstructed in 3D by meshing the pelvic surface with a segmentation software called Materialize Mimics. Then, the 3-Matic processing software is used to improve meshing and extract the data needed to carry out all the measurements in this study. Then, Matlab programming is used to compare the hemi-pelvises, in terms of volume, surface area, distance from the plane of symmetry and deviation of the surface. Finally, the influence of age and sex of patients on the properties of pelvic symmetry is explored.

KEYWORDS : CT scan images, pelvis, surgical planning, symmetry, 3D models, deviation analysis.

SOMMARIO

Questa tesi di Master mira ad aiutare i chirurghi ortopedici nel trattamento delle fratture del bacino utilizzando una placca di osteosintesi. Per produrre una placca specifica per il paziente prima del intervento e facilitare il processo di pianificazione chirurgica, vengono sviluppati modelli virtuali in 3D del bacino a causa della sua complessa struttura ossea. In questo modo, la modellazione aiuta a capire le caratteristiche della frattura e a ridurre la durata dell'intervento chirurgico, e quindi il rischio di sanguinamento. Inoltre, migliora i risultati post-operatori immediati e a lungo termine.

Attualmente, questi modelli utilizzano l'emi-pelvi sano controlaterale per visualizzare l'emi-pelvi fratturato prima della frattura. Di conseguenza, si presuppone una perfetta simmetria del bacino. Inoltre, la valutazione clinica del trattamento chirurgico si basa su criteri come il sistema di notation di Matta, che prevede anche la simmetria del bacino. Tuttavia, i cambiamenti morfologici legati all'età e al sesso possono portare a un'asimmetria pelvica. In particolare, la parte inferiore del bacino maschile e femminile si evolve in modo diverso, a causa di funzioni biologiche come il parto per le donne. È quindi fondamentale determinare se il bacino può essere considerato simmetrico o meno per costruire l'immagine virtuale 3D del bacino pre-frattura.

In questo lavoro, gli strumenti di modellazione sono utilizzati per confrontare le simmetrie globali e locali del bacino. Pertanto, le somiglianze nelle regioni di interesse (definite dal chirurgo ortopedico) sono analizzate sulla base di immagini TC raccolte da una coorte di 28 pazienti con bacino sano. Le immagini vengono ricostruite in 3D mappando la superficie del bacino con un software di segmentazione chiamato Materialize Mimics. Successivamente, è stato utilizzato il software di elaborazione 3-Matic per migliorare la mesh ed estrarre i dati necessari per eseguire tutte le misurazioni di questo studio. È stata poi utilizzata la programmazione Matlab per confrontare gli emibacini in termini di volume, area superficiale, distanza dal piano di simmetria e deviazione superficiale. Infine, è stata esplorata l'influenza dell'età e del sesso del paziente sulle proprietà della simmetria pelvica.

PAROLE CHIAVI: immagini TC, pelvi, pianificazione chirurgica, simmetria, modelli 3D, analisi della deviazione.

RESUME EN FRANÇAIS

Ce travail de Master Thesis vise à aider les chirurgiens orthopédiques dans le traitement des fractures du bassin qui utilisent une plaque d'ostéosynthèse. Afin de fabriquer en préopératoire une plaque spécifique au patient et faciliter le processus de planification chirurgicale, des modèles virtuels de bassin en 3D sont développés dû à la structure complexe du bassin osseux. Ainsi, la modélisation aide à comprendre les caractéristiques de la fracture et à diminuer la durée de l'intervention chirurgicale, et donc le risque de saignement. Elle améliore les résultats post-opératoires immédiats et à long terme.

Aujourd'hui, ces modèles utilisent l'hémi-bassin controlatéral sain pour visualiser l'hémi-bassin fracturé avant la fracture. Par conséquent, une symétrie parfaite du bassin est admise. En outre, l'évaluation clinique du traitement chirurgical est basée sur des critères tels que le système de notation de Matta, qui implique également la symétrie du bassin. Cependant, les changements morphologiques liés à l'âge et au sexe peuvent entraîner une asymétrie du bassin. Notamment, les bassins masculins et féminins évoluent différemment, dû aux fonctions biologiques telles que l'accouchement pour les femmes. Il est donc crucial de déterminer si le bassin peut être considéré comme symétrique ou non pour construire l'image virtuelle 3D du bassin fracturé avant la fracture.

Dans ce travail, des outils de modélisation sont utilisés pour comparer les symétries globales et locales du bassin. Par conséquent, les similitudes dans les régions d'intérêt (définies par le chirurgien orthopédique) sont analysées sur la base d'images de tomodensitométrie recueillies auprès d'une cohorte de 28 patients dont le bassin est sain. Les images sont reconstruites en 3D en maillant la surface du bassin avec un logiciel de segmentation appelé Materialize Mimics. Ensuite, le logiciel de traitement 3-Matic est utilisé pour améliorer le maillage et extraire les données utiles pour effectuer toutes les mesures de cette étude. Ensuite, la programmation Matlab est utilisée pour comparer les hémi-bassins, en termes de volume, de surface, de distance par rapport au plan de symétrie et de déviation de la surface. Enfin, l'influence de l'âge et du sexe des patients sur les propriétés de la symétrie pelvienne est explorée.

MOTS-CLÉS : Images de tomodensitométrie, bassin, planification chirurgicale, symétrie, modèles 3D, analyse des déviations.

LIST OF FIGURES

LIST OF TABLES

MEDICAL AND TECHNICAL TERMS

Acetabulum: the deep, cup-shaped structure that encloses the head of the femur at the hip joint.

Anatomical reduction: the surgical treatment realized by an orthopedic surgeon to align almost perfectly the bone fragments or the dislocated joint in relation to their normal anatomical position (<1 mm). However, a difference of position <2 mm is considered as a good reduction.

Controlateral: the opposite side of an object.

Osteosynthesis: procedures used to repair fractures or mechanical problems of bones, by fixing these latter in their original anatomical position so that they can heal properly.

Osteosynthesis plates: medical devices used in orthopedic surgery to stabilize and support broken bones during the healing process. They are typically made of metal (like stainless steel or titanium) and are attached to the bone with screws.

Rigid transformation: transformation of a set of points using only translation, rotation and scaling.

Surgical intervention: the treatment which involves cutting of tissues or closure of a previously sustained wound.

Surgical planning: the preoperative method of pre-visualizing a surgical intervention, in order to predefine the surgical steps and any bone segment repositioning in the context of the final outcome.

ACRONYMS

AP: antero-posterior (axis)

BMI: BioMechanics/BioEngineering

CAD: Computer-aided design

CNRS: National Centre for Scientific Research

CPD: Coherent Point Drift

CT: Computed Tomography (scan)

DCM: deviation color maps

ISM: Institute of Movement Sciences

IUT: Institute of Technology

MIPS: Mirror image with regard to the plane of symmetry

ML: medio-lateral (axis)

ORIF: Open reduction with internal fixation

PSO: Percutaneous screw osteosynthesis

RMS: Root Mean Square

RTA: Road traffic accidents

SD: standard deviation

SI: sacroiliac (joints)

SMI: Bio-inspired Systems

THA: Total hip arthroplasty

THR: Total hip replacement

-

INTRODUCTION

The pelvis is a fundamental anatomical structure of the human body because it plays a crucial role in trunk support, locomotion and the transmission of loads between the trunk and the lower limbs, as well as in human obstetrics. The geometric symmetry or asymmetry between the left and right sides of the pelvis is of particular interest, not only from an anatomical point of view, but also in the context of medical science, anthropology and biomechanics.

In the context of medical science, the main purpose is the reduction of pelvis fractures by conventional surgery. Therefore, internal fixation is used after exposure of the fracture, representing an invasive and time-consuming procedure. As a result, patients are exposed to increased risk of morbidity and mortality. To avoid post-operative complications, accurate fracture reduction is crucial. However, the geometric complexity of the human pelvis, particularly in acetabular fractures, makes it difficult to assess and manage injuries in the event of trauma. Precise knowledge of the symmetries and asymmetries of the pelvis would be a valuable asset for diagnosis, choice of equipment and assessment of a good reduction.

The best response to pelvic fracture is reduction using patient-specific osteosynthesis plates. These ones are created pre-operatively with computer-aided design (CAD), with the aim of decreasing surgery time, increasing fracture understanding and thus decreasing the risk of bleeding, and improving immediate and longer-term post-operative results. To facilitate the surgical planning process and develop these patient-specific osteosynthesis plates, 3D virtual pelvis models are being developed. Currently, these models use the healthy contralateral side of the pelvis to visualize the fractured (pre-injury) side, assuming perfect symmetry between the two sides of the pelvis. In addition, clinical assessment of reduction is based on criteria such as the Matta scoring system, which involves symmetry of the pelvis. However, age-related morphological changes could have an impact on symmetry. Similarly, differences between male and female pelvises, linked to the biological requirements of each sex, such as childbirth in women, could also lead to differences in symmetry.

Modelling tools are used in this master thesis work to compare global and local symmetries. Therefore, similarities in areas of interest defined by the orthopedic surgeon are analyzed on the basis of CT scan images collected from a cohort of 28 patients. Segmentation software called Materialize Mimics is used on CT scans of the pelvis of healthy patients to reconstruct it in 3D, by meshing the pelvic surface. Firstly, the volume and surface area of both sides of the pelvis are compared. Then, the 3-Matic processing software is used to improve meshing and extract the data. In addition, as the pelvic fracture involves the acetabulum, its spherical shape is compared between the left and right

sides using 3-Matic processing software. Symmetry is studied both as a mathematical property in relation to a plane of symmetry and geometrically by aligning surfaces. Therefore, the Matlab programming platform is used to generate the plane of symmetry (first step) and then to align geometrically (second step) the two sides of the pelvis. The surface deviations are calculated after the first step as well as after the second one, and they are compared. Finally, this study explores the influence of age and sex of patients on the properties of pelvic symmetry.

This master thesis manuscript is divided into 7 parts. First, the research center where this study is carried out, is described. Then, the first and second chapter of the manuscript concern the context of this work and a description of the associated literature. Firstly, the anatomy and the functions of the pelvis permit to highlight the complexity of the study. Secondly, the treatments of acetabular fractures, their planning, the type of operations, the equipment used and the complications that may be encountered, are described. This part aims to show how this study can help the work of orthopedic surgeons. Therefore, the main point is to validate the symmetry of the pelvis, which will enable the fractured side of the pelvis to be visualized as it was before the injury, knowing the healthy side. Hence, surgeons are the first beneficiaries of these results. In the third chapter concerning the materials, all the numerical tools used in this study are presented. Their choice is explained as well as the limitations encountered. Then, the fourth chapter details the methods and algorithms developed in this master thesis work to treat CT scan images of the 28 healthy patients selected: 3D segmentation of images with the software Mimics; data extraction with the software 3-Matic, after standardizing the mesh and reaching spherical shape for the acetabulum; development of Matlab algorithms to define the plane of symmetry, to align the hemi-pelvises and to quantify the symmetry between them. In the fifth chapter, results of the methods and algorithms used in this work are presented and analyzed. The discussion of the sixth chapter comprises the contribution to the treatment of acetabular fractures according to age and sex of patients and the comparison with literature. Finally, the last chapter concerns the conclusion and the perspectives of this master thesis, introducing the extension of this work as part of a doctoral thesis that is starting in the research center of Institute for Movement Sciences of Aix Marseille Université (France).

THE RESEARCH LABORATORY

The “Etienne-Jules Marey Institute of Movement Sciences” (ISM) is a Joint Research Unit (UMR 7287), under the co-administration of Aix-Marseille University and the French National Centre for Scientific Research (CNRS). The laboratory comprises about 150 members (CNRS researchers, teacher-researchers, Engineers, technicians and PhD students).

The laboratory is located in several sites of Marseille (see figure below):

- in the Campus of Luminy
- in the Hospital Sainte-Marguerite
- in the Faculty of Medicine near the Hospital Timone
- in the Institute of Technology (IUT) of Aix-en-Provence.

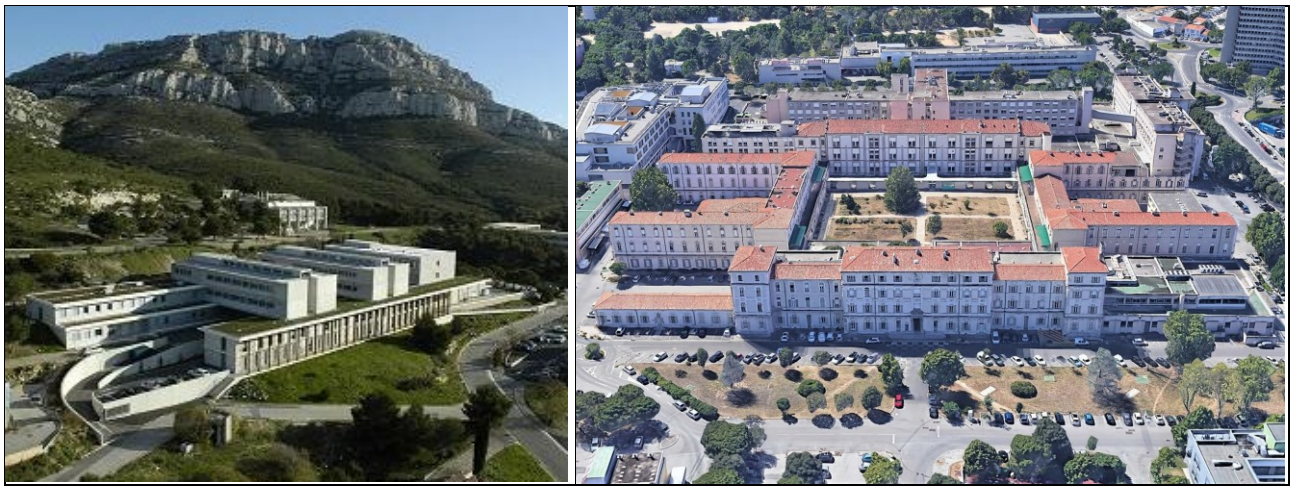

Figure. Sites of the “Etienne-Jules Marey Institute of Movement Sciences” :
(left) in the Campus of Luminy and (right) in the Hospital Sainte-Marguerite.

Over the last ten years, the ISM has developed expertise in multidisciplinary approach to movement analysis. Convinced that the understanding of movement cannot be based solely on the identification of standardized determinants, the ISM is interested in an integrative approach to highlight their dynamic interactions. The ‘movement system’ is a new central paradigm that guides research at the ISM around three essential themes:

- structural elements underlying movement, drawing on biomechanics, material and movement science concepts
- sensory-motor, cognitive and psychological processes and determinants
- bio-inspired modelling applied to the design and control of moving systems

Three teams constitute the laboratory ISM:

- Team 1: The **BioMechanics/BioEngineering (BMI)** team develops interdisciplinary scientific projects on the tissues of the osteoarticular and musculoskeletal systems and their interactions with movement.

- Team 2: **The Behavioral and Cognitive Dynamics team (DynamiCC)** team aims understanding movement through interactions between different disciplinary approaches such as experimental and social psychology, behavioral and cognitive neuroscience, and neurophysiology. The projects concern animals as well as humans, from both individual and group perspectives.

- Team 3: The **Bio-inspired Systems (SBI)** team proposes scientific breakthroughs from the understanding of living systems to engineering innovation. A wide range of topics is studied with a biomimetic approach: insect flight, osteogenesis, joint morphogenesis, flexible joints, biological actuators or perceptual and cognitive processes in animals.

Consequently, the laboratory is renowned at the level of material biomechanics and motion sciences (constitutive domain of team 1), psychology, neurophysiology and behavioral and cognitive neurosciences (constitutive domain of team 2) and bio-inspired robotics (constitutive domain of team 3). The approach is systemic, with the notion of chain value, whether disciplinary, multidisciplinary or interdisciplinary, right through to its applications in the fields of health, sport, education, robotics and transport. This approach also provides a multi-scale perspective: from micro to macro, from cell to tissue and whole body, from animal to human, from human to robot (and vice versa). These two key points are essential and constitute the main strength of the ISM research paradigm. To support its projects, the ISM has acquired high-tech specialist equipment ranging from miniaturized embedded sensors and precision tools to customized all-inclusive experimental environments. In addition, the ISM has five technological platforms.

- The Centre de Réalité Virtuelle de la Méditerranée (CRVM) is at the forefront of the study of human movement through interactive immersive techniques, and is a resource center renowned for its scientific and industrial applications.

- The Aix-en-Provence Technology Platform encourages innovation and technology transfer in the field of (bio)mechanics.

- The Flight Arena is built for research in Biorobotics.

- The MECABIO platform provides a service to the benefit of patients, by enabling mechanical characterization of biological and bio/materials.
- The TechnoSport is created to associate high-level sport with scientific research with a view of both improving the performance of athletes, and also to improve health and quality of life of the most vulnerable populations (obese, elderly).

The research at ISM is also supported by long-term corporate partnerships through university chairs:

- with Decathlon for sports equipment
- with Stellantis for automotive industry
- with AG2R to design training situation tests to prevent the risk of falling and the decline of cognitive-motor functions.

To sum up, the size of ISM, the variety of researchers' disciplines and their originality give it a unique position at national and international level.

The Master's thesis work is carried out within the team BMI, which studies healthy, pathological and repaired osteoarticular and musculoskeletal systems by an integrated multidisciplinary, multi-scale and multi-physics approach marked by strong links between biomechanists, biologists, biomaterials specialists and clinicians. The team's work focuses on bone regeneration, tissue degradation and re-shaping dynamics, imaging, biomechanical adaptations to stress, individual studies of movement and surgical aids.

In this context, the aim of this work is to contribute to the surgical treatment of pelvic fractures. Therefore, this work is supervised by Martine Pithioux, the supervisor of this thesis, head of ISM. and Marie Le Baron, orthopedic surgeon at Hôpital Sainte-Marguerite.

I. Anatomy of the pelvis

This master thesis focuses on the properties of symmetry of the pelvis to help orthopedic surgeons for a more effective management of acetabulum fractures. It is therefore necessary to provide an anatomical description of the bony pelvis and other tissues of the pelvis, its functions and anatomical reference points.

I.1. Bone anatomy

The bony pelvis is a complex structure that forms the base of the trunk and supports the abdominal organs. It is composed of three main types of bone (**Figure 1**):

- **The coxal bones (or iliac bones):** one on each side constituted by three parts that fuse together in adulthood, namely the ilium, ischium and pubis.
- **The sacrum:** triangular in shape and located at the base of the spine, it articulates with the two iliac bones to form the sacroiliac joint.
- **The coccyx:** this is the end of the spine and lies just below the sacrum.

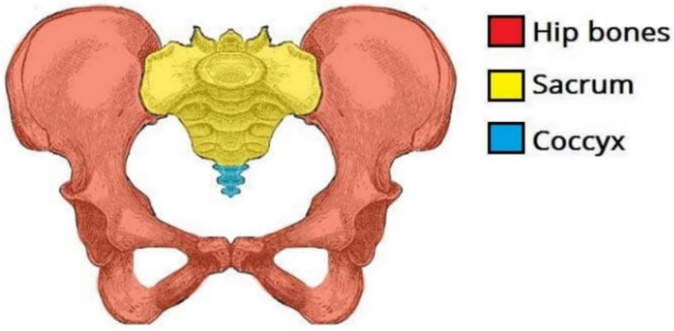

Figure 1. Different parts of the pelvic bones.[2]

Each pelvis bone is itself composed of three parts (**Figure 2**), which fuse together in adulthood:

- **The ilium** is the upper and widest part of the pelvis bone. It forms the iliac crest, which can be felt under the skin on the sides of the waist.
- **The ischium**, located below and behind, forms the lower part of the pelvis, in particular the ischial tuberosity, on which we sit.
- **The pubis** is the lower anterior part of the pelvis bone. The two pubic bones meet at the front to form the pubic symphysis, a cartilaginous joint.

The bony pelvis forms a rigid and sloping ring with two large apertures:

- **The upper strait** (or upper aperture of the pelvis): This is the entrance to the pelvis, which is bordered by the upper edge of the pubis at the front, the wing of the ilium at the sides and the promontory of the sacrum at the back.

- **The lower strait** (or lower aperture of the pelvis): This is the outlet of the pelvis, bounded by the pubic arch in front, the ischial tuberosity on the sides and the coccyx in the back.

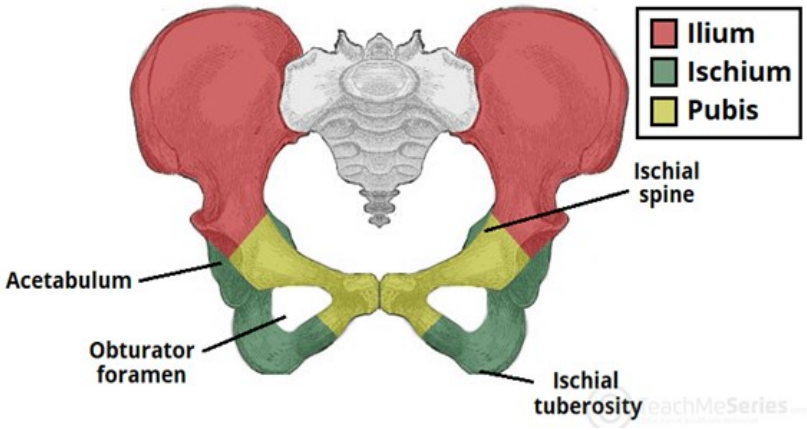

Figure 2. The three parts of the pelvis bone.[3]

I.2. Other tissues of the pelvis

The pelvis is held together by several joints:

- **The lumbosacral symphysis** consists of all the joints that join the lumbar rachis to the sacrum. They are cartilaginous, with a vertebral disc between vertebrae L5 and S1 and two synovial joints. The longitudinal anterior/ventral ligament, which covers the vertebrae up to the anterior face of the sacrum, strengthens the lumbosacral symphysis. In addition, two ligaments attach vertebra L5 to the sacrum: the lumbosacral ligament and the iliolumbar ligament (**Figure 3**).

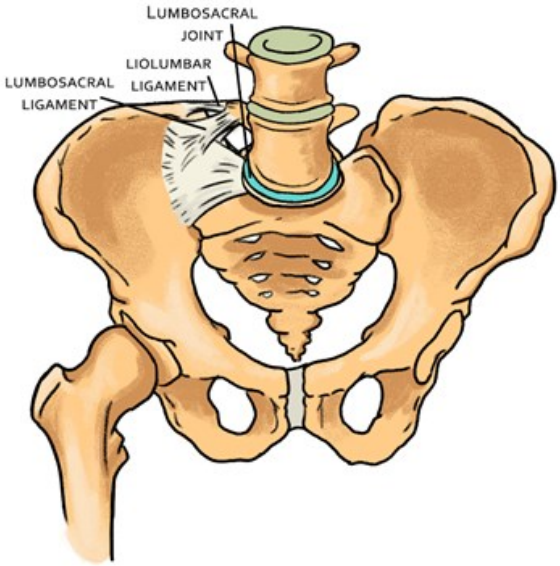

Figure 3. The lumbosacral symphysis.

- **The sacroiliac joints** (SI): These synovial joints connect the right and left iliac bones to the sacrum and are strongly stabilized by a joint capsule and 3 types of ligaments: the anterior sacroiliac ligaments, the posterior sacroiliac ligaments and the interosseous ligaments (**Figure 4**).

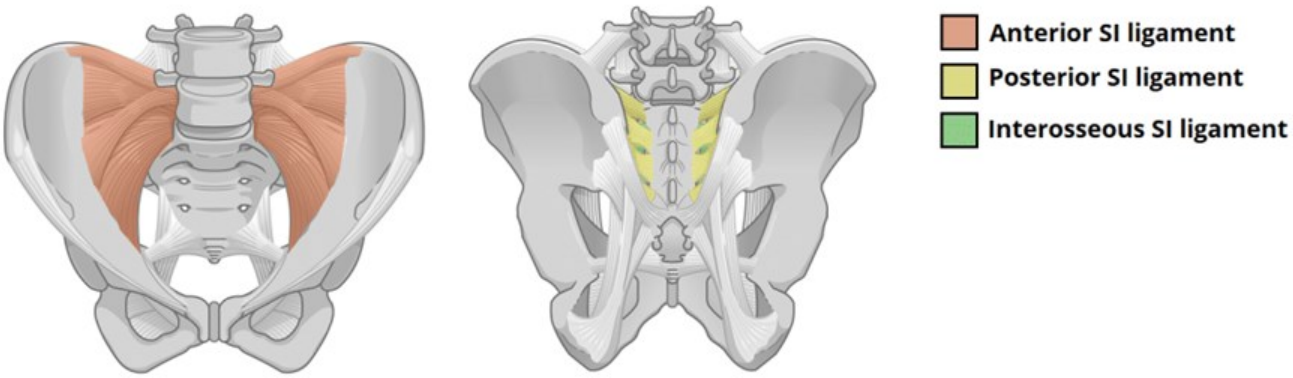

Figure 4. The ligaments of the sacroiliac joints.

- The pubic symphysis is a cartilaginous joint made of fibrocartilage and held in place by the upper and lower pubic ligaments (**Figure 5**).

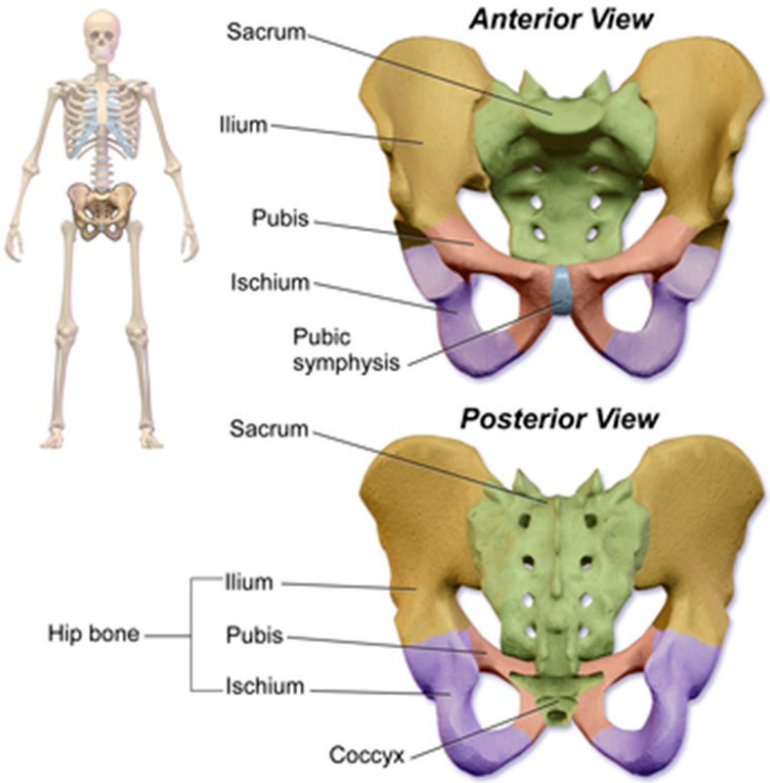

Figure 5. The pubic symphysis.

- **The coxofemoral joints** connect the head of the femur to the acetabulum of the pelvis as shown in Figure 6. The acetabulum is a cavity deepened by the presence of a fibrocartilaginous collar, called the acetabular labrum, into which the head of the femur is inserted. Both the acetabulum and the femur are covered by articular cartilage, which is thicker where weight is borne. In addition, a series of ligaments maintains stability between the two bony tissues.

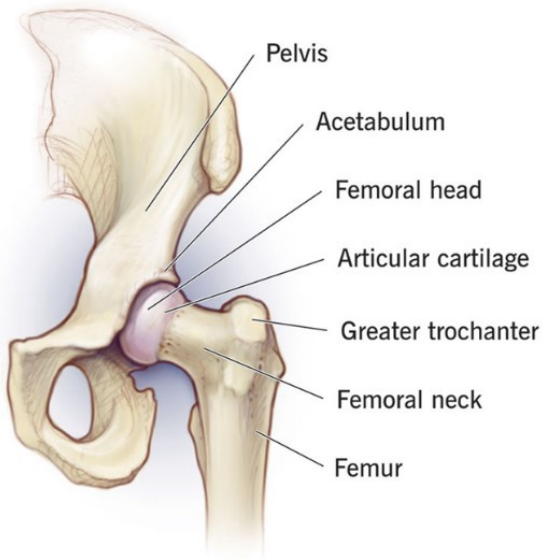

Figure 6. The coxofemoral joints.

Although not used in our study, the presence of these joints will help to explain certain unexpected results.

I.3. Functions of the pelvis

The role of the pelvis is manifold:

- **Protection** of the pelvic cavity containing the bladder, the reproductive tract for men and the vagina and uterus for women, and the rectum.
- **The support and transmission** of axial forces (weight) in bipodal support, as the pelvic belt skeleton supports the spine and connects the trunk to the lower limbs (Figure 7). It provides a balanced distribution of weight from the trunk to the lower limbs, as well as of the reaction of the ground to this weight. These forces meet at the coxofemoral joints.

- **Insertion** of muscles, nerves, arteries and veins such as the sciatic nerve, the longest nerve in the human body, which can be damaged in the case of dislocation of the femoral head.

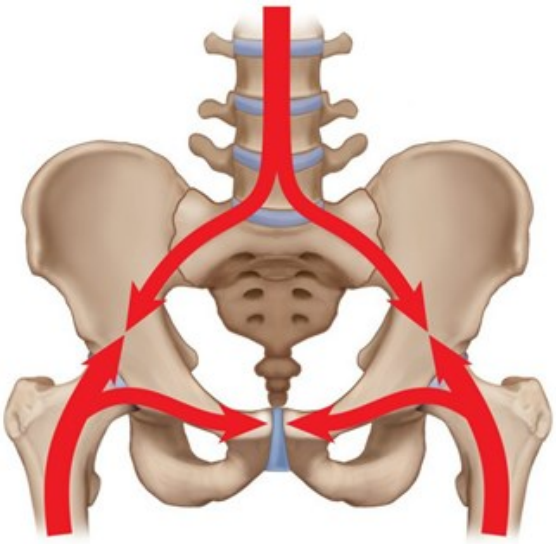

Figure 7. Diagram of force transmission in bipodal support.[4]

In short, the bony pelvis is a robust and complex structure, essential for 1) movement, 2) posture and 3) protection of internal organs. Damage to the pelvis can endanger any of these three functions and should be diagnosed as early as possible.

I.4. Anatomical reference points

As the basin displays a complex 3D shape, 3 orthogonal planes (one in relation to the other) are used to describe it (Figure 8):

- **The coronal (or frontal) plane** corresponds to the front view of the body in the anatomical reference position. It divides the body into two parts: an anterior part (front) and a posterior part (back). The axis perpendicular to this plane is called the antero-posterior (AP) axis. A structure located in front of this plane is called anterior, while a structure located behind it is called posterior.
- **The sagittal plane** divides the body into two halves, left and right, and allows a profile view. The axis perpendicular to this plane is called the medio-lateral (ML) axis. A structure that is close to the sagittal median plane (which divides the body into two symmetrical parts) is called medial, and a structure that is further away from it is called lateral.

- **The axial (or transverse) plane** gives a top view and divides the body into two parts: an upper part (upwards) and a lower part (downwards). The axis perpendicular to this plane is the superior-inferior (SI) axis. A structure located towards the top of the body is said to be superior, while a structure located towards the bottom is said to be inferior.

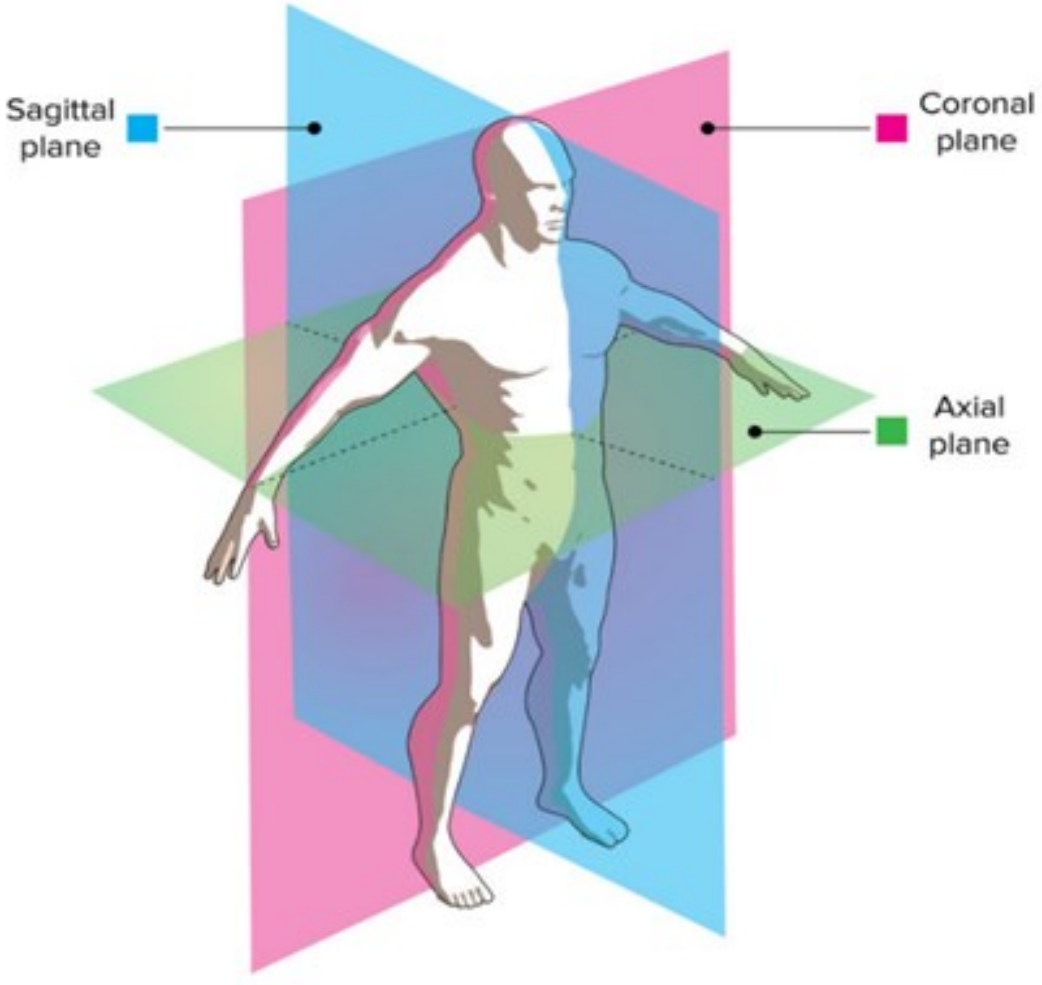

Figure 8. The three orthogonal cutting planes used on scanners.[5]

In addition, the terms ‘proximal’ and ‘distal’ are used to describe the relative position in relation to the point of attachment or origin of a structure on the trunk. A proximal part is closer to this point of attachment, while a distal part is further away. These different concepts will help to describe the overall anatomy of a structure and will be used throughout the study for a better spatial understanding.

II. Acetabulum fractures treatments

The surgical treatment of acetabulum fracture is still difficult to treat according to literature. In addition, it leads to a high morbidity rate of up to 24% for patients aged over 70[6]. The first descriptions of this fracture date back to Ancient Egypt in 5000 BC, with rudimentary treatment using pieces of wood and bandages. However, the intensive development of acetabulum fracture treatment took place in the second half of the twentieth century, following the seminal work of Judet and Letournel[7,8]. Hence, Letournel classification of fractures, their causes, surgical and non-surgical treatments and post-operative complications are explained in this chapter. Then, measurements of pelvis symmetry are related to modern surgical aids used by certain orthopedic surgeons.

II.1 Classification of acetabulum fractures

In modern medicine, it is necessary to classify the different fractures of the pelvis. This makes it possible to predict the surgical approach, as well as its management. In the case of this study, the classification gives an idea of the regions of interest for the orthopedic surgeon. In France, the most widely used classification system is that of Judet-Letournel, in which the specific fracture patterns are grouped into 10 subsets (Figure 9).[7,9] These latter depend on the mechanism of the injury, the vector of application of the force during injury, the anatomy of the bone and its mechanical properties.

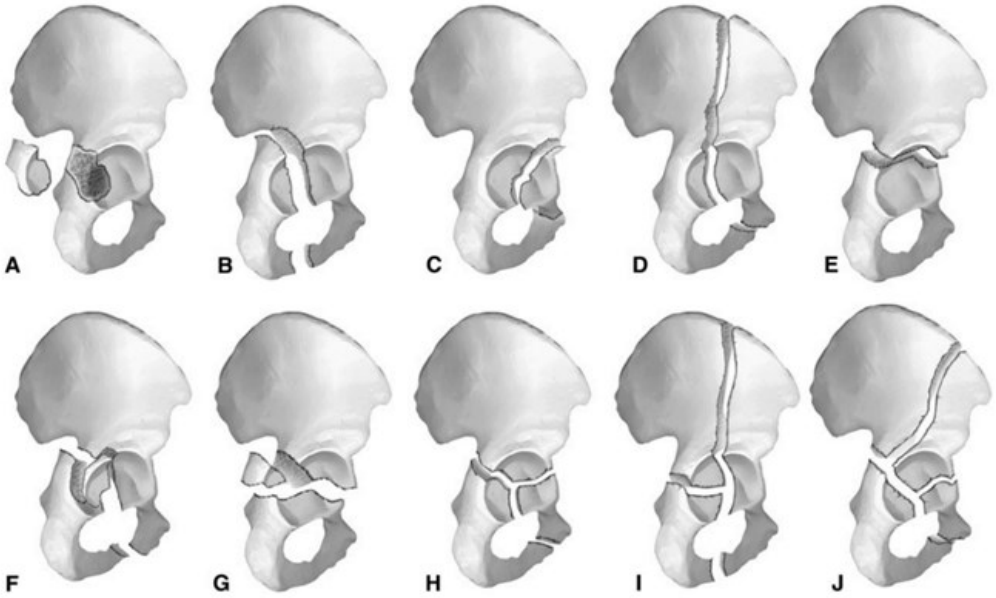

Figure 9. Letournel classification into 10 subsets.[9]

The 10 subsets (A to J in Figure 9) correspond to two types of fracture (Table 1):

Simple fractures	Complex fractures
A : posterior wall	F : posterior column with a posterior wall
B : posterior column	G : transverse posterior wall
C : anterior wall	H : T-style
D : anterior column	I : anterior column posterior hemitransverse
E : transverse	J : both columns

Table 1. The 10 types of fracture in the Letournel classification (shown in Figure 9).[9]

According to this classification, the most common acetabular fractures are posterior wall fractures, two-column fracture, and transverse fractures associated with posterior wall fractures, which account for more than 70% of acetabular fractures (Table 2).

	Letournel and Judet et al.[10]	Matta et al.[11]	Dakin et al.[12]	Ohashi et al.[13]	Jindal et al.[14]
Case (No.)	567	255	85	73	120
Posterior wall	22.4	8.6	12.9	27.7	28.3
Posterior column	2.3	3.1	1.2	4.1	4.2
Anterior wall	1.6	1.2	1.2	0	7.5
Anterior column	3.9	4.7	1.2	4.1	10.8
Transverse	3.7	3.5	8.2	8.2	13.3
Posterior column with a posterior wall	3.5	3.9	18.8	9.6	5.0
Transverse posterior wall	20.6	23.5	35.3	20.5	5.0
T-style	5.3	12.2	3.5	11.0	11.7
Anterior column posterior hemitransverse	8.8	5.9	3.5	6.8	1.7
Both columns	27.9	33.3	14.1	11.0	12.5

Table 2. Frequency distribution in percentage of acetabular fractures in different reports.

This classification provides a preoperative planning system, which is used to determine the most appropriate surgical approach. At the time of the original description, acetabulum fractures were not commonly treated by open surgery, which often led to pain and post-traumatic arthritis. Letournel found that reducing the articular surface improved clinical outcomes and reduced the development of arthritis.[10] He evaluated that the rate of arthritis decreases from 30.7% in imperfectly reduced cases to 5.4% in anatomically reduced cases. Patient follow-up ranged from 2 to 21 years, with 75.7% having a very good outcome.[11] However, although he divided fractures into 10 subsets, Letournel noted that acetabulum fractures represented a broader spectrum of injury, as incomplete fracture lines

and combined fracture patterns were common. In addition, this classification is purely anatomical, and in no way prejudges the relative severity of the different lesions, the difficulty of surgery, or the prognosis. Thus, despite its usefulness, fracture treatment still depends very much on the experience of orthopedic surgeons. Indeed, the recent study (2024) by Yücens et al. demonstrated that, according to the experience of surgeons and the types of approach, this classification is not sufficient to describe acetabulum fractures, as combined fracture patterns are frequent and some fractures cannot be classified in these subsets.[15]

There are other classifications such as those of Bulcholz[16], Young and Burgess[17] or Tile-AO[18] (Arbeitsgemeinschaft für Osteosynthesefragen). This latter is the most widely used internationally. It groups all pelvic fractures related to the major forces producing the lesions and their stability. However, this classification is based more on the severity of the injury and less on the anatomical description of the lesions like Letournel classification. This is why, in the anatomical study of pelvic symmetry, Letournel classification is preferred to that of Tile-AO. Consequently, it must be noted that due to the complexity of pelvic anatomy and the specificity of fracture types, treatment is not only patient-specific, but also surgeon-specific, due to the inadequacy of existing classifications.

II.2. Causes of the acetabulum fractures

Initially, acetabulum fractures were caused by high-energy impacts. Among these high-energy traumas, the majority of cases recorded are road traffic accidents (RTA) and falls from a height (> 1m) (**Table 3**).

	Case (No.)	Mean age (year)	RTA (%)	Fall from height (%)	Other (%)
Gianoudis et al.[19]	1667	39 ± 5	80.5	10.7	8.8
Dias et al.[20]	126	40 ± 4	78	12.4	9.6
Kumar et al.[21]	73	40	64.4	24.7	9.9
Jindal et al.[14]	116	40 ± 16	72.4	21.6	6
Heeg et al.[22]	54	34	96.3	0.7	0
Brueton et al.[23]	40	38	75.0	22.5	2.5

Table 3. Epidemiology of high-energy fractures of the acetabulum (*RTA = Road Traffic Accident).*

However, over the last few decades, there has been a significant increase in the incidence of acetabular fractures in elderly patients. This is explained by longer life expectancy and higher activity levels in this age group. Because their bones are more fragile, the elderly patients are prone to low-energy fractures, most often due to a simple fall (<1m), as shown in the table 4. In a study conducted by Boudissa et al. on 414 patients over 10 years (2005-2014) in France, the distribution of acetabulum fracture origins was found to be 25% due to low-energy trauma and 75% due to high-energy trauma.[24] In addition, a third of patients had a multiple fracture.

	Case (No.)	Mean age (year)	Fall from standing height (%)	Fall from height (%)	RTA (%)	Other (%)
Tissingh et al.[25]	19	77	63.2	10.5	15.8	10.5
Rickman et al.[26]	24	77	87.5	8.3	4.2	0
Kim et al.[27]	186	70	30.1	19.4	40.8	9.7
Heimke et al.[28]	41	75	70.7	14.6	14.7	0
Albrektsson et al.[6]	2132	~76 (median)	56	12	18	14

Table 4. Epidemiology of acetabulum fractures in the elderly population (> 60 years) (*RTA = Road Traffic Accident).*

Between 2014 and 2020, Albrektsson et al. studied the causes, the mortality and the treatments carried out on 2,132 cases of acetabulum fracture in Sweden. High-energy fractures affected 21% of patients, 47% of whom were under 70 years old. Low-energy fractures, on the other hand, accounted for 63% of fractures in general and 94% in patients aged over 70. Finally, the study found that the average time between fracture and osteosynthesis was 5 days. Severe acetabulum fractures are often of concern to orthopedic surgeons, as they require patient-specific surgical treatment plans and customized equipment.[6]

II.3. Treatment of acetabulum fractures

Diagnosis of acetabular fracture is based on visual examination of the patient lesions, but above all on medical imaging, which comes from X-rays and CT scans. The visualization of characteristic landmarks on 2D images enables the orthopedic surgeon to identify the type of fracture, based on the Letournel classification seen previously (Fig. 9 and Table 1).

II.3.1 Characteristic landmarks on 2D images

The planes of the characteristic landmarks on the 2D images are given in Table 5.

Anterior landmarks	Landmarks in No man's land	Posterior landmarks
Anterior wall of the acetabulum	Roof of the acetabulum	Posterior wall of the acetabulum
Iliac wing	Quadrilateral blade	Posterior edge of the iliac wing
Anterior edge of the iliac wing	Obturator frame	

Table 5. The characteristic landmarks on 2D images.

It must be noted that undamaged landmarks are just as important as landmarks affected by a lesion. Depending on the type of fracture and on the age of the patient, the orthopedic surgeon can make a diagnosis and decide on the type of treatment.

II.3.2 non-surgical treatment

Non-surgical treatment consists of either skeletal traction for 3 weeks with passive mobilization of the pelvis (Figure 10), or simple bed rest followed by active and passive mobilization without weight bearing for a total of 6 weeks. Once the bone has healed sufficiently to prevent displacement during movement, the patient can begin physical therapy to rehabilitate the pelvis for movement. However, it is important in this case to follow up regularly with a physical examination and X-rays images to ensure that the fracture remains in the correct position and is healing properly. Then, healing can take 3 to 4 months.

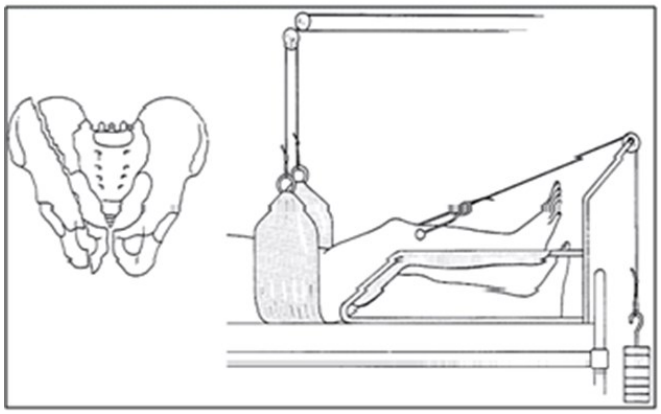

Figure 10. Assembly of a skeletal traction of the pelvis[29]

This type of treatment is recommended for small fractures that are not displaced by movement. It may also be recommended for elderly patients or those with serious medical problems, for whom surgery would be too risky.

II.3.3. Surgical treatment

Surgical treatment is invasive and three methods have been defined in the literature for acetabulum fractures:

Method 1: Open reduction with internal fixation (ORIF) is the standard method for treating a fracture of the acetabulum. The orthopedic surgeon makes an incision close to the fracture site to access the bone, reposition the broken parts and fix them with osteosynthesis plates and screws. This Surgery involves several key steps:[29]

1) Pre-operative planning: detailed assessment on X-rays and scans to determine the type of fracture and plan reduction.

2) Patient positioning: Usually supine (patient lying on his or her back with head/neck/trunk aligned). Skeletal traction may be added if it helps to realign the bones.

3) Surgical approach: The incision and approach depend on the type of fracture. Common approaches include:

- Modified Stoppa approach (Figure 11A and 11B)
- Ilioinguinal approach
- Kocher-Langenbeck approach (Figure 11C and 11C)

Several of these approaches can be used for a single ORIF, as shown in figure 11.

4) Fracture reduction: The bone fragments are repositioned in their anatomical alignment using various instruments.

5) Internal fixation: Metal plates and screws are used to maintain the reduction. Common configurations include:

- Suprapectinal and infrapectinal reconstruction plates
- Interfragmentary compression screws
- Quadrilateral wall support plates1

6) Radiological control: Intraoperative X-rays are taken to check reduction and positioning of the equipment.

7) Closing: closing plan by plan with possible drainage.

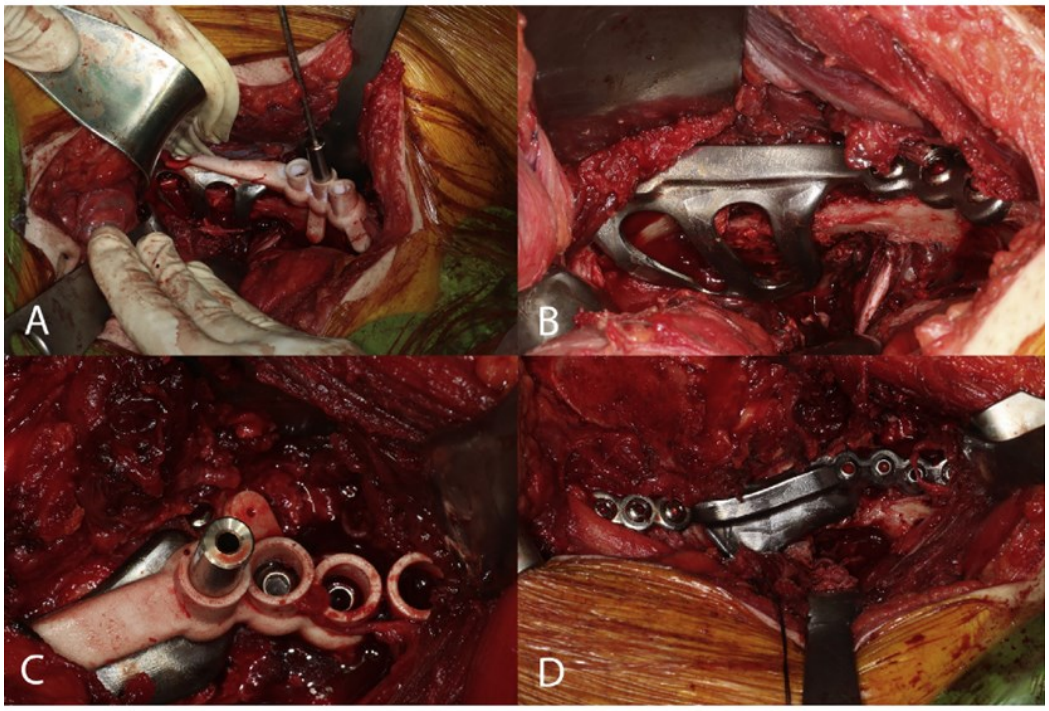

Figure 11. Surgical approach images of an ORIF for a both column fracture of the left acetabulum: (A and B) a Stoppa approach with a clear view of the anterior plate, which is placed over the pelvic rim; (C and D) a Kocher-Langenbeck approach with a clear view on the posterior.[1]

This is the therapy of choice for displaced fractures that cannot be treated non-surgically, especially in the case of young patients. Even in the case of older patients (aged between 65 and 104), Rommens et al.[30] showed that excellent short-term results, even though 24% of the patients had to undergo total hip arthroplasty as a second surgical treatment (described below).[30–32]

Method 2: Total hip arthroplasty (THA) or total hip replacement (THR) involves replacing the acetabulum and the femoral head with two interlocking prostheses that enable the functions of the damaged tissues (that cannot be recovered) to be maintained. The prosthesis consists of the femoral stem connected to the femoral head, which is fixed in the femur. This femoral head is made of metal or ceramic (Figure 12). A cup is screwed into the acetabulum, the cavity in the pelvis where the head of the femur is housed, once all the remaining cartilage has been removed. This cup is usually made of metal with the inside of the cavity made of polyethylene (plastic). In many cases, a reduction (open or not) is necessary in order to fix the bone stably and restore the general shape of the acetabulum in order to implement the acetabular prosthesis. Modalities to minimize dislocation include the use of larger femoral heads and dual mobility cups.[26,33–35]

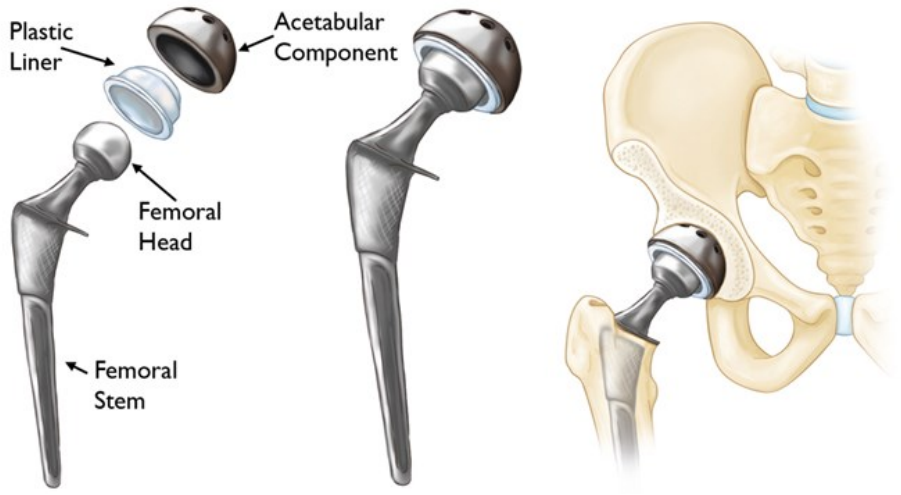

Figure 12. The components of a total hip prosthesis[36]

Patients are considered for THA if any of the following criteria are met:

- Existing or post-traumatic arthritis
- Avascular necrosis of the femoral head post-operatively
- Osteoporotic bone for elderly patient
- Multiple fractures associated with the femoral head that do not allow a good result with ORIF alone
- Poor result at an early stage during follow-up after ORIF.
- In elderly patients requiring early mobilization

Method 3: Percutaneous screw osteosynthesis (PSO) involves making an incision just above the fracture to insert screws (Kirschner wires) to fix the two pieces of the bone that have been separated. Anesthesia can be local or general. The advantage of local anesthesia over ORIF is that it reduces soft tissue disruption, operating duration, blood loss and post-operative pain. However, the fracture must be simple and only slightly displaced. The technique enables earlier return to activity and better pain control in comparison with nonsurgical management.[37–39]

Albrektsson et al. showed that among the 2,132 patients registered, a quarter (503) required screw osteosynthesis plates or prostheses, involving ORIF, THA or both (Figure 12).[6]

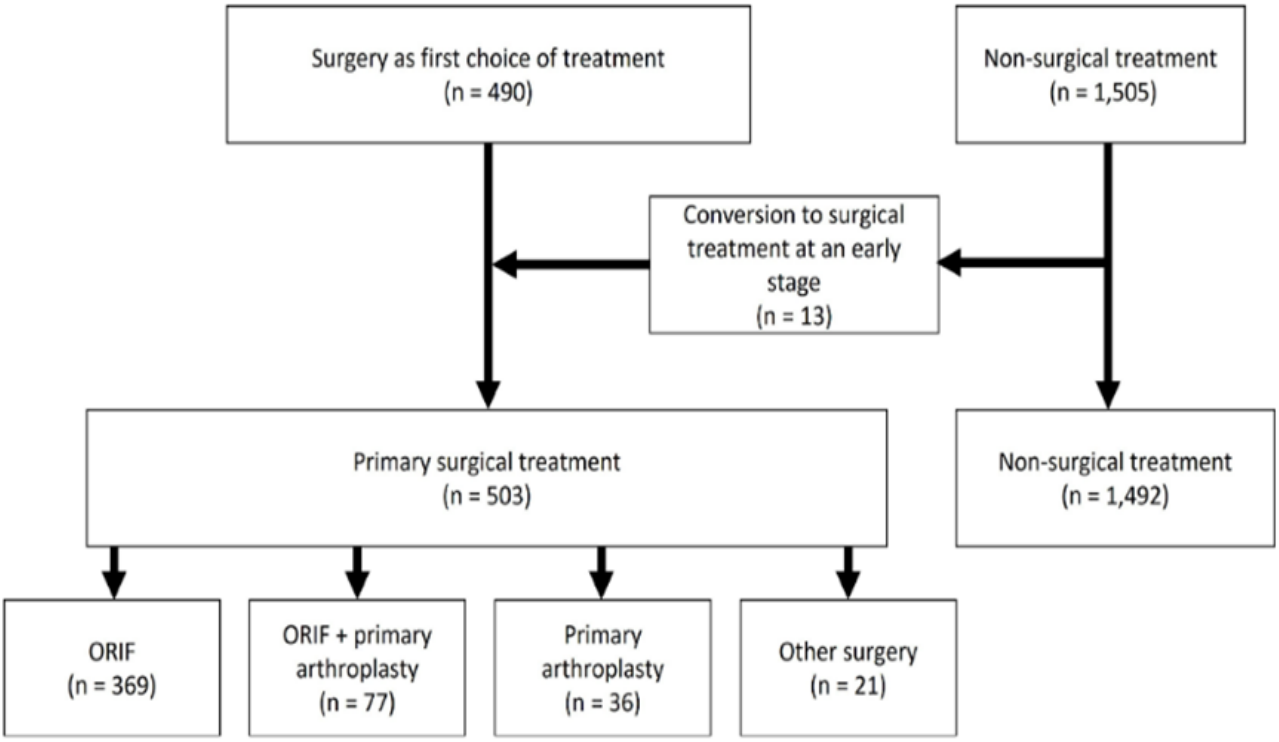

Figure 14. Fracture management according to Albrektsson et al. for 2132 patients.[6]

Both prostheses and screw osteosynthesis plates must be adapted as closely as possible to the anatomy of the bone. The success of the treatment depends on a number of criteria to ensure that the bone is not displaced more than 2mm from its initial position. In the case of simple fractures of the acetabulum, the treatment is well known and highly studied. However, the treatment of complex fractures of the acetabulum is difficult as they affect different parts of the acetabulum. In addition, the existing classifications may not be sufficient to easily plan the operation. The orthopedic surgeon's expertise is therefore the only guarantee that post-operative complications can be avoided.

Finally, numerous studies have confirmed the importance of surgical treatment less than two weeks after the accident, and even 5 days for associated fractures.[21,23,40,41] In addition, Madhu et al. estimated that the probability of obtaining an anatomical reduction decreased by 18% for each day spent without treatment even for simple cases.[40]

II.4. Post-operative complications

There are many risks associated with surgery, both short-term and long-term ones:

- **Hemorrhage:** The surgical operation requires the incision of soft tissue to reach the fracture site, resulting in blood loss. This loss increases with the duration of the operation.
- **Sciatic Nerve Palsy (SNP):** As the sciatic nerve is close to the incision or fracture zone, it can be partially or totally severed either during the incision or during the placement of the osteosynthesis material. This leads to sensory and motor problems in the lower limb.
- **Infection:** As with any surgical procedure, there is a risk of infection following the incision.
- **Deep vein thrombosis (DVT)**: Prolonged immobilization of the patient during and after surgery increases the risk of blood clots forming in the deep vein. These clots may also be due to the detachment of cartilage or bone marrow, which is then found in the veins after the fracture. They generally lead to pain, varicose veins and, in the worst cases, pulmonary embolism.
- **Pulmonary embolism (PE):** This is a potentially fatal complication, resulting from a blood clot travelling up the pulmonary artery. The clot is usually bony or cartilaginous, due to fracture.
- **Arthritis:** Post-traumatic arthrosis of the pelvis, known as coxarthrosis, is a frequent long-term complication, even when the fracture is anatomically reduced. It can develop up to 25 years after the operation and results in pain and reduced mobility.
- **Joint stiffness:** Despite the re-education that follows surgery, a limitation in pelvis mobility may persist.
- **Heterotopic ossification**: Surgical intervention requires manipulation of the soft tissue surrounding the fracture, causing trauma and local bleeding. This trauma, together with the presence of the osteosynthesis material, provokes an inflammatory reaction that stimulates abnormal bone formation. Muscle tissue changes into a calcified bone structure, leading to a considerable restriction of mobility in the joint.

The table 6 shows the frequency of these post-operative complications according to the literature[10,11,14,21,42–46] except for arthritis, joint stiffness and heterotopic ossification because they may require a very long-term monitoring.

Complications	Case (No.)	Mortality (%)	Deep vein thrombosis (%)	Pulmonary embolism (%)	Sciatic Nerve Palsy (%)	Infection (%)	Failure of Fixation (%)
Letournel and Judet et al.[10]	569	2.3	3	2.1	2	4.2	1
Matta et al.[11]	259	NR	NR	NR	12	5	3
Mears et al.[42]	100	1	5	1	5.33	4	1
Routt et al.[21]	108	NR	NR	3	5	3	NR
Helfet et al.[43]	84	0	6	4	5.17	0	2
Giannoudis et al.[19]	84	3	4.3	NR	2.05	4.4	NR
Kumar et al.[21]	72	0	0	0	1.4	4.01	1.4
Gupta et al.[44]	63	0	NR	NR	3.1	7.93	1.5
Jindal et al.[14]	120	4.1	3.3	2.5	1.16	6.6	1
Lundin et al.[45]	72	NR	2.6	5.7	NR	3.9	1.7
Deo et al.[46]	79	1	3	9	NR	4	4

Table 6. Frequency of post-operative complications according to the literature.

To reduce these post-operative risks, a thorough knowledge of the patient's pelvic bone anatomy prior to surgery is an asset. Firstly, it allows more accurate restoration of normal anatomy, which is essential to minimize the risk of post-traumatic coxarthrosis. In addition, accurate anatomical reduction promotes better long-term joint congruence. Secondly, this knowledge facilitates optimal incision and placement of the osteosynthesis material, making it possible to avoid high-risk areas such as the path of the sciatic nerve or the iliac vessels, while ensuring stable fixation. Finally, a detailed understanding of the anatomy helps to reduce the duration and invasiveness of the surgery. These factors are known to increase the risk of infection. In short, a thorough knowledge of the patient's pelvic anatomy allows the orthopedic surgeon to operate more efficiently, accurately and safely, reducing the risk of major post-operative complications.

II.5. Modern surgical aids

Modern techniques have been developed to provide a thorough knowledge of the patient's pelvic bone anatomy and assist the orthopedic surgeon. The aim is to plan the surgical operation in advance and to evaluate post-operative result, using 3D numerical models or physical models produced by 3D printing:

- **3D digital models**: Image processing software enables orthopedic surgeons to move from a 2D study of the fracture site, using X-ray or CT images, to a 3D study. The 3D CT-scan provides a complete three-dimensional view of the fracture and the surrounding anatomy, as well as greater freedom in manipulating the image to examine the fracture from all angles. In terms of pre-operative analysis, this provides more accurate measurements of displacements and gaps between bone fragments and precise quantification of the total area of the gaps, giving a better idea of the extent of displacement. In terms of post-operative assessment, it provides accurate measurements of the reduction as well as detection of minimal residual displacements that may be missed in 2D.[47,48]

- **3D physical models:** based on the 3D digital models, 3D physical models can be manufactured using 3D printing. Ideally, the fractured side should be reproduced as a flexible 3D object, made up of pieces of bone with artefact-free fracture lines, as mentioned by Weidert et al.[49] Thus, the fracture would be better visualized and it could be manipulated safely before surgery to see how to reunite the pieces of bone and achieve the best anatomical reduction. Then, the osteosynthesis plate used to reattach the pieces of bone together could be folded in an optimized way, so that it could then be sterilized and used directly during the surgery. However, creating a flexible 3D model, made up of pieces of bone, is much more time-consuming and expensive than a rigid one-piece model. This is why the technique used today is the “mirror technique” by printing the contralateral healthy hemi-pelvis of the fractured hemi-pelvis. Therefore, the patient's contralateral healthy hemi-pelvis is used as a model to prepare the osteosynthesis plates, assuming that the pelvis is perfectly symmetrical.[49–51]

Today, the “mirror technique” is used by certain orthopedic surgeons to train pre-operatively (Figure 14). The method is detailed by Upex et al. in the case of a fracture of both columns.[50] The aim is to:
- Reduce the duration of the operation: a time saving of around 30 minutes has been observed.
- Improve precision: pre-molded plates facilitate anatomical reduction of the fracture.
- Reduce adjustments during surgery: no additional intraoperative casting is generally required.

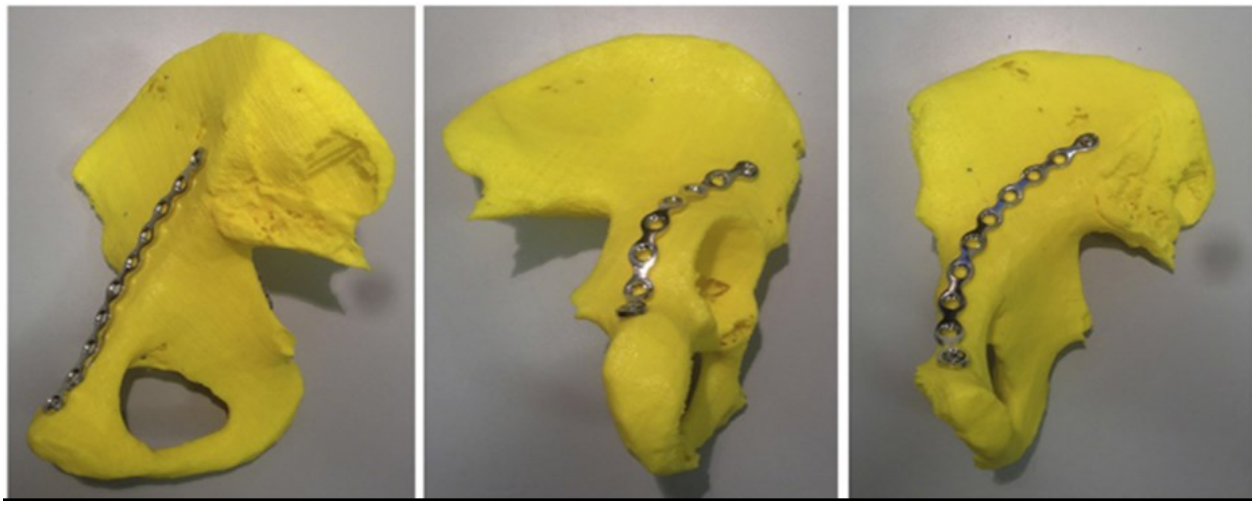

Figure 15. 3D printing of the patient's contralateral healthy hemi-pelvis in the "mirror technique" with pre-molded osteosynthesis plates.[50]

The materials often used for 3D printing of the hemi-pelvis are the polyactic acid material and the acrylonitritebutadiene styrene thermoplastic material, whose average costs and printing times are listed in Table 7. These factors depend not only on the material but also on the 3D printer used and the 3D resolution of the object.[49–51]

	Average cost of material (€)	Average printing time (min)	Time saved in surgery (min)
Weidert et al.[49]	**5**	**520**	**12.7**
Upex et al.[50]	**6**	**1440**	**30**
Rodriguez et al.[51]	**12**	**385**	**NA**

Table 7. Average costs, printing times of hemi-pelvis 3D printing and time saved in surgery.

Finally, orthopedic surgeons, especially younger and less experienced ones, can profit from training using virtual procedure and 3D models. Therefore, the pelvis is assumed to be perfectly symmetrical, which justifies the use of the contralateral healthy hemi-pelvis to prepare the osteosynthesis plates.

II.6 Existing methods for measuring pelvic symmetry

The pelvis is a bone with a complex geometry. Hence, it is very difficult to 'measure' its symmetry (or asymmetry). A study was carried out by Boulay et al. on 12 healthy pelvises of patients (cadaveric pelvises) with an average age of 72.6 years in order to measure their degree of asymmetry. 71 variables were measured on each hemi-pelvis according to common reference points and 56 of them were symmetric. To determine the reproducibility of these measurements, different experiments were carried out:

- To test intra-observer reliability using the Fastrak system, the same pelvis was measured six times using a subset of 39 landmarks; each time, it was set at the same position on its support.
- To test inter-observer reliability using the Fastrak system, the same pelvis was measured by two different observers.

To measure the asymmetry, they used a dimensionless asymmetry index, for each variable. The advantage of using a dimensionless unit is that we are no longer dependent on the real value of the variable or the size of the pelvis. However, the disadvantage is that the clinician does not evaluate his surgery in terms of differences in percentages but in terms of match/mismatch with dimensions (millimetres). Finally two types of error were observed during this study: a systematic error related to the position of a point and a random error related to the pointer.[52]

The advent of CAD software made it possible to study the symmetry from 3D scanners of the pelvis. Therefore, Ead et al.[53] and Zheng et al.[54] proposed a new method to examine the entire 3D geometric shape of the pelvis.

They used CT scans of the pelvis to convert into 3D models, "mirror" each side of pelvis (hemi-pelvises) and aligned the right hemi-pelvis with the left one. They studied CT scans of (nbre) patients and they calculated the deviation for each set of hemi-pelvises models: the root mean square of the deviations were of 1.14 ± 0.26 mm and 1.15 ± 0.16, respectively. And the average percentage of points below a deviation threshold of ± 2mm were of 91.9 ± 5.55% and 90.82 ± 4.67, respectively. They represented the deviations in a deviation color maps (DCM) which showed that the largest deviations were on non-articular surfaces (figure 16).

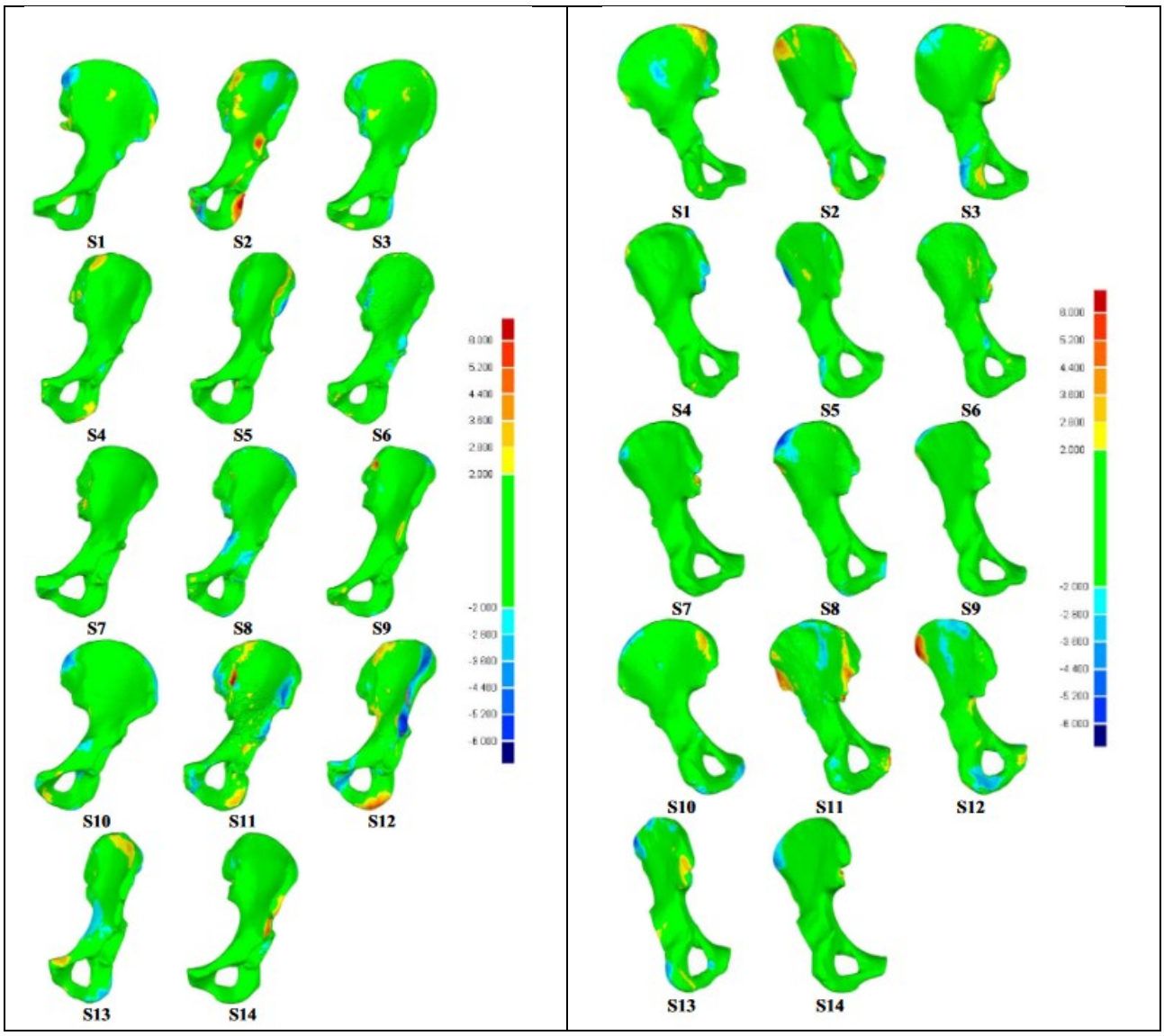

Figure 16. Anterior view (left) and posterior view (right) deviation color maps (mm) of the left side and reflected right side of the pelvises.[53]

In the literature, the volume and surface area of each hemi-pelvises were also investigated. These works showed no significant differences between the left and right sides, indicating that the pelvis is bilaterally symmetrical. However, authors define the property of symmetry of the pelvis on the basis of a global correspondence between the mirror image of one hemi-pelvis and its contralateral. In addition, these studies only use one of the hemis-pelvis aligned with its contralateral. Therefore, they assume that the alignment algorithm would give the same result on both sides, whereas the mesh may be different for the two hemi-pelvises.[53,54]

In conclusion, the previous studies on pelvic symmetry found in the literature guided at the starting of this master's thesis by providing the advantages and limitations of their methods:

- Using CAD software makes it possible to study the 3D geometry of the pelvis from 3D scanners, which are easier to access than cadaveric pelvises.
- Dimensionless measurements are very useful for comparing the two hemi-pelvises but must be accompanied by measurements with dimensions for a better understanding by the surgeon.
- A great deal of attention must be paid to the methods of meshing and aligning the hemi-pelvises.
- The process must be automated as much as possible in order to reduce human error and obtain similar results when repeating measurements on the same pelvis.
- The influence of parameters such as age and gender must be taken into account in order to determine their influence on symmetry.

III. Materials

The aim of this master thesis is to study the symmetry of the pelvis using CT scans taken on healthy patients. The first requirement is to be able to use the scanner images to obtain a 3D visualization of the pelvis for further measurements. Therefore, Materialise Mimics software, used in the literature for segmentation, seems to be an appropriate choice. Then, manipulating the reconstructed pelvis and extracting data is enabled by 3-Matic software. As the algorithms used in these two software packages are not open source and display limitations, Matlab platform is used for operation on data, measurements and statistical analysis.

III.1. CT scan images

III.1.1. Principle

The Computed Tomography scan (CT scan) is an imaging modality used by orthopedic surgeons for diagnostic. A conventional scanner is a tube in which the patient lies on a sliding table (Fig. 15).

Figure 17. Computed Tomography (CT) scanner.[55]

The X-ray sources are placed as fan-shaped (Fig. 18).[60] Facing these sources are detectors, each of which captures the rays at a given angle. This source/detector pair is rotated while the patient is moved through the tube as the source rotates. The rotation is therefore helical, enabling the structures to be imaged over a certain length. The imaging process takes around 15 minutes.

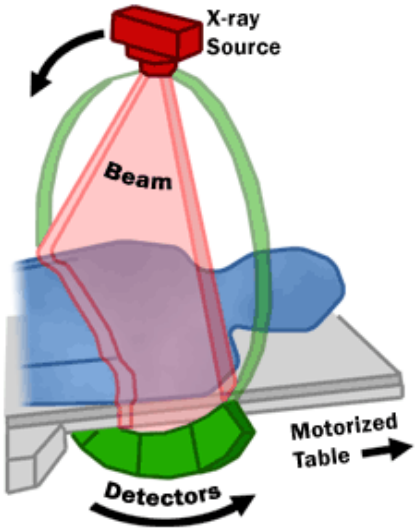

Figure 18. CT fan beam and patient in a CT imaging system.[60]

The X-ray attenuations by different tissues inside the body are measured. The multiple X-ray measurements taken from different angles are then processed on a computer using tomographic reconstruction algorithms to produce tomographic (cross-sectional) images (virtual "slices") of a body: the information is processed in the form of matrices (sinograms) by the computer and then translated into grey-scale coded images.

The main advantage of CT scan is that it provides three-dimensional images by combining data collected from the three anatomical planes of space (frontal, sagittal, axial). Thus, it leads to detailed internal images of the body, dividing the different tissues into more than 4,000 different grey levels depending on their density. In this way, unlike ultrasound, the body can be viewed in depth with good resolution.

III.1.2. Calculation of Density

The grey levels are given in a unit called the Hounsfield Unit (HU). Its value is calculated as a function of X-ray absorption coefficient in the penetrated tissue (μ_{tissue}) and that of the water (μ_{water}), using the formula:

$$HU = 1000 \times \frac{\mu_{tissue} - \mu_{water}}{\mu_{water}} \qquad [1]$$

The Hounsfield scale ranges from -1000 for air to +3000 for the densest bone tissue.[61] The formula above places water at 0 HU while spongeous bone starts at around 200 (Figure 19).

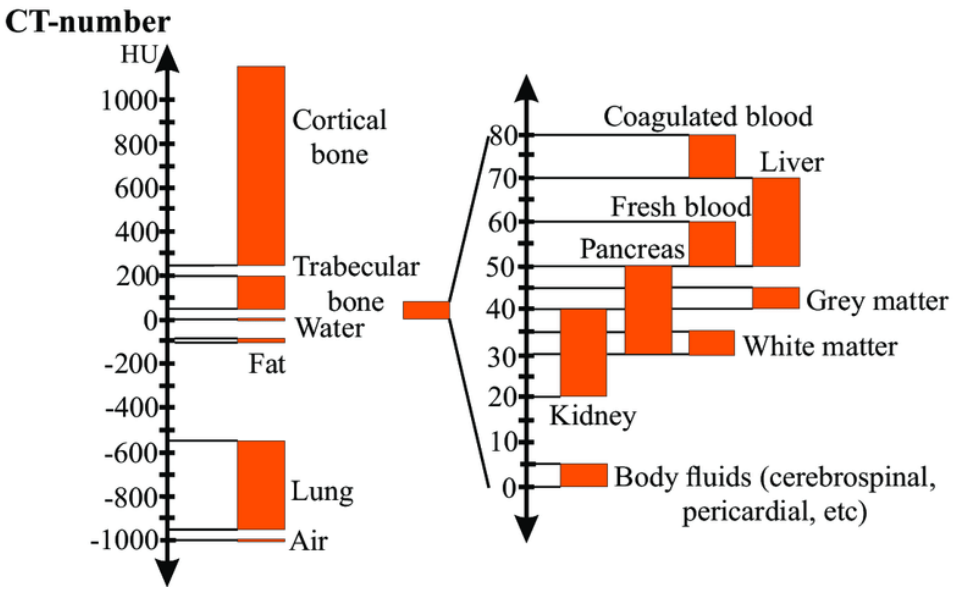

Figure 19. The Housfield scale for different kind of tissues.[61]

This scale is the first means used to separate bone from the rest of the average tissue when processing scans. However, it must be pointed out that spongeous bone (due to osteoporosis, for example) can be at the same level of HU as joints, such as ligaments, and so becoming a source of error.

III.1.3. Parameters for high quality images

Images are displayed in the 3 anatomical planes seen above, each perpendicular to an axis (X, Y or Z) defined from the 3D reference frame of the scanner. Therefore, the image voxels (3D pixels) have coordinates in this frame of reference, enabling them to be located in space and so to represent the body in 3D, thanks to all the slices taken in each of the planes. Before image acquisition, three important parameters need to be set to ensure good quality scans and optimal 3D reconstruction:

- **Slice thickness** is related to the step of the helix that the ring describes around the patient. It defines the size of the voxels and therefore the resolution of the images. This resolution depends on the acquisition parameters, but also on the size of the receptors. Hence, the resolution cannot be less than the size of the scanner detectors.
- **Filters** can be used to modify the contrast of the images depending on the tissues to be visualized: bone or soft tissue.
- **Contrast products** can be used to visualize vessels. However, it should be noted that even if these contrast products give better visualization, they also change the densitometry values on the images, and so inducing errors.

Bones are clearly visible on CT images and this is the preferred 3D imaging modality for bones (Figure 20).

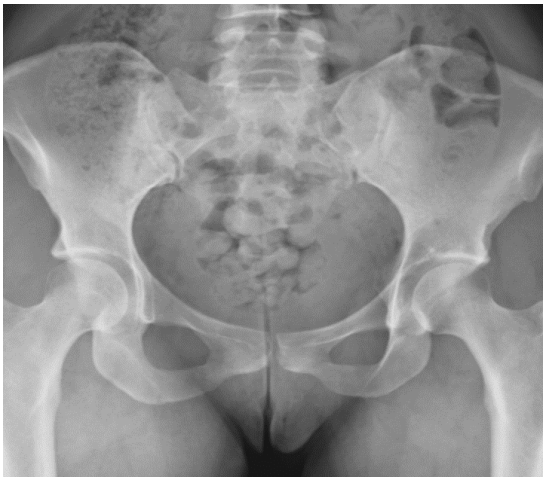

Figure 20. CT scan image of a female pelvis (front view).[6]

III.1.4. Scanning mode for the pelvis

A CT scan of the pelvis is performed in cases of pain, trauma, falls, suspected osteoarthritis or dysplasia (tissue malformation) of the pelvis. As mentioned above, a CT scan provides 2D images in all 3 planes of space. However, given the anatomical complexity of the pelvis, performing a frontal scan only (Figure 20) may result in a loss of information. In order to avoid superimpositions of bones, additional images taken from an oblique view provide clearer and more detailed perspectives for accurate diagnosis by the orthopedic surgeon (Figure 21):

- **The ¾ alar or internal oblique approach** (Figure 21.1) involves turning the patient 45° outwards from the healthy side and allows study of the iliac wing, sacroiliac joint, posterior column and anterior border of the acetabulum.
- **The ¾ obturator or external oblique approach** (Figure 21.3) involves turning the patient 45° outwards in relation to the affected side and allows the acetabulum, anterior column and obturator framework to be studied.

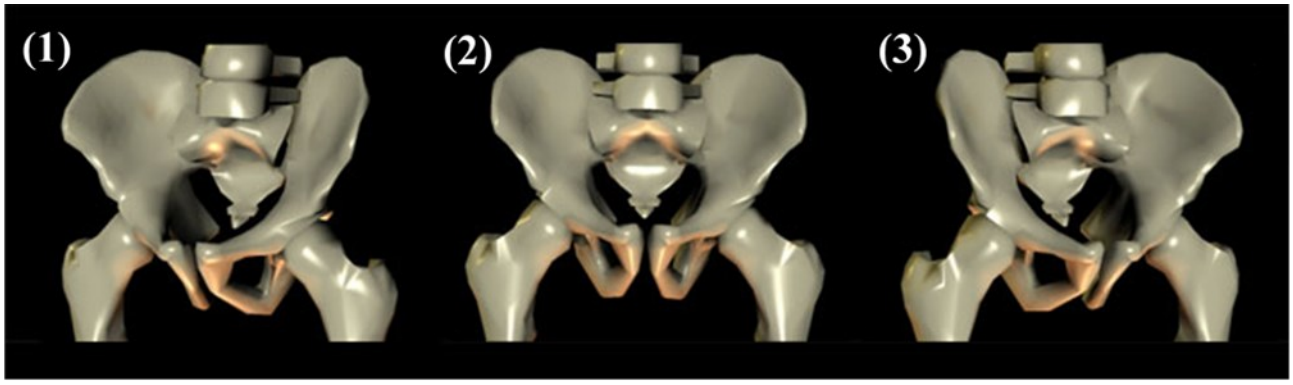

Figure 21. A pelvis seen (1) from the ¾ alar view, (2) from the front and (3) from the ¾ obturator view, assuming a right-sided lesion.

Reference lines are drawn by the orthopedic surgeon on each of these views (face, ¾ alar and ¾ obturator), as it will be defined in the following section. Thus, the surgeon can define the type of fracture, choose the appropriate approach and osteosynthesis material based on the radiographic projection of the fracture, prior to direct visualization of the lesion in the operating room. However, it must be pointed out that in the case of 3D visualization of the pelvis after reconstruction from CT scan images, these reference lines are not as appropriate as in 2D.

III.2. Materialize NV software

The software used in this work comes from the Belgian company Materialize NV, which specializes in the design and distribution of advanced additive manufacturing technologies, software for medical applications and custom 3D printing services. The company offers a complete range of innovative solutions in the field of digital manufacturing and personalized healthcare. The company is particularly interested in the creation of virtual 3D anatomical models to facilitate surgical planning, and in the development of 3D printing for the design and precise placement of screws for custom implants. In particular, the company has developed the aMace Acetabular Revision System, which uses a fully patient-specific approach to the development of acetabular implants using:

- detailed 3D analysis of the pelvis using CT scans of the patient
- assessment of bone loss by experienced clinical engineers
- implant design to perfectly match the patient's anatomy

Their support for these steps is a digital platform that facilitates collaboration between clinical engineers and orthopedic surgeons, and 3D printing of drill guides for screw placement.[56]
As the aim of this Master thesis work is to provide a useful study for orthopedic surgeons to help in planning acetabulum fractures treatment, the Materialise NV software proved to be very suitable for studying the pelvis bones. In addition, the laboratory ISM has licences for Mimics and 3-matic, which are used throughout this work.

III.2.1. The software Mimics for 3D segmentation

The software Materialize Mimics 3.0 is used in this work for 3D segmentation of medical images produced by computed tomography (CT), magnetic resonance imaging (MRI), radiography and ultrasound. It converts series of 2D images obtained in DICOM format into 3D models, by reconstructing the surface of their anatomical structure. Image segmentation is an image processing operation consisting of detecting and assembling pixels according to criteria, as intensity or spatial ones. The aim is to make the image appear with uniform regions corresponding these criteria. In this work, segmentation uses input images to produce masks that isolate and label the different anatomical structures, on each slice of the CT data. These masks can then be used to reconstruct appropriate 3D models by triangulating the external surfaces of the identified regions. In pelvis study, the masks need to isolate the bones of the pelvis.

III.2.2. The software 3-matic for data extraction

Once the two hemi-pelvises are reconstructed with segmentation on CT scan images, data are extracted for the study of pelvis symmetry. Therefore, the most appropriate software used is 3-matic 15.0. It is a 3D optimization software designed specifically for 3D printing and additive manufacturing in the medical field. It has useful tools for modifying and optimizing 3D meshes, applying textures, patterns and transforming 3D objects, converting meshes into CAD formats and preparing data for simulation.

III.3. The use of Matlab for measurements

MATLAB (an abbreviation of "MATrix LABoratory") is a proprietary multi-paradigm programming language and numeric computing environment developed by MathWorks. MATLAB allows matrix manipulations, plotting of functions and data, implementation of algorithms, creation of user interfaces, and interfacing with programs written in other languages. In this work, Matlab R2023a algorithms are used to perform measurements on data exported from 3-Matic.

IV. Development of methods and algorithms

For this master thesis work, a procedure is first defined for the selection of CT scan images of 32 healthy patients but 4 of them have unusable data (poor resolution, segmentation too tedious, etc.). The average age is 55.5 ±20 years old with a range of 22-84 years old. The series is split equally between men and women (14 of each). Then, these images are treated with 3D segmentation, defining a process in several steps in the software Mimics. Finally, data are extracted with the software 3-Matic, after standardizing the mesh so that the two hemi-pelvises can be compared and reaching spherical shape for the acetabulum. The aim is to obtain a digital 3D representation of the pelvis that resembles as closely as possible to reality. Finally, Matlab algorithms are developed to define the plane of symmetry, to align the hemi-pelvises and to quantify the symmetry between them.

IV.1. Selection of CT scan images

CT Scan images of Thoraco-Abdomino-Pelvic (TAP) are imported in DICOM format on CDs. They are mainly provided by the hospital Sainte-Marguerite, but also from the military hospital LAVERAN and the European hospital of Marseille. In these CDs, the most interesting series of images are then selected, i.e. those that will give the best quality pelvis after segmentation and mesh processing.

It must be pointed out that for the starting of this study, the patients are selected on the basis of the absence of pathologies on the pelvis or changes in it (tumors, lesions, prostheses). All of the images concern the Thoraco-Abdomino-Pelvic (TAP) and they have been realized on patients suffering from other pathologies such as scoliosis (Figure 21).

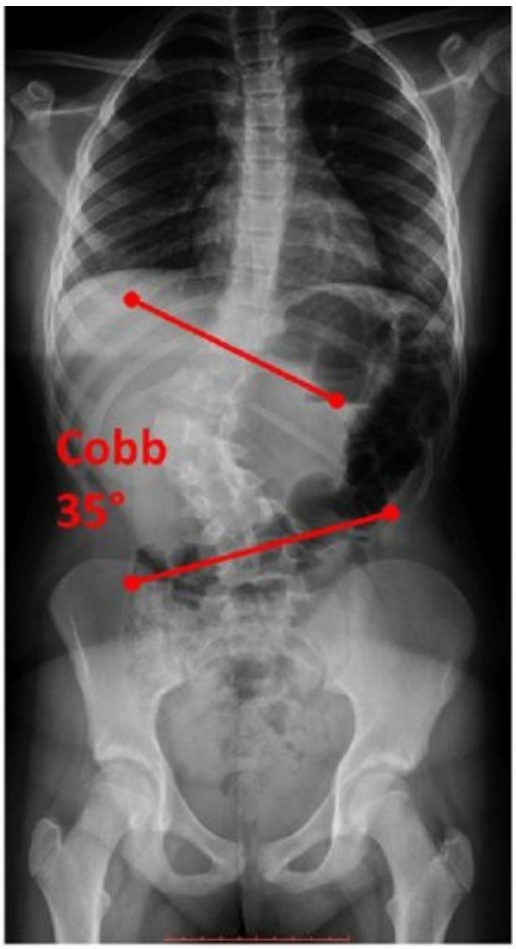

Figure 21. CT scan of a patient suffering from scoliosis with a healthy pelvis eligible for this study.[57]

IV.2. Steps of 3D Segmentation with Mimics

In this Master thesis work, a large number of repeated trials are necessary with Mimics to establish the six processing steps required to obtain a digital 3D representation of the pelvis, that resembles as closely as possible to reality.

IV.2.1. Thresholding

Thresholding is a method involving the manual definition of a density threshold, here in Hounsfield units (equation [1] and Fig. 17), in order to keep only the tissues of interest. The minimum threshold value for bones is 226 HU on mimics (default value defined by the software). The result of the threshold displays regions that do not belong to the bone (Figure 20). A large proportion of these voxels are due either to noise related to imaging parameters or to the presence of the surgical table.

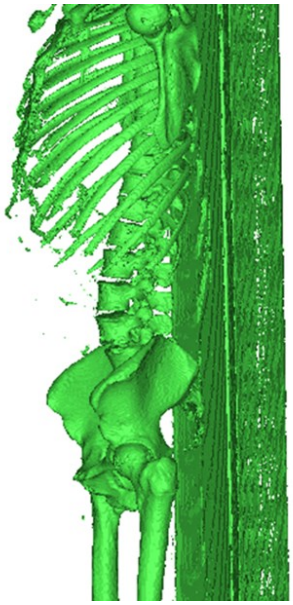

Figure 23. 3D scan of the patient after the thresholding step.

It must be pointed out that several parameters such as the scanner parameters, the properties of the bone and the noise generated during image capture, make perfect selection impossible. Therefore, for practical reasons (better separation of the bones during the subsequent steps), the range used in this work varies from patient to patient but remains around HU of 226-3000. The maximum difference calculated between the pelvic surface using a patient-specific interval [200-3000] and the default Mimics interval for bone (which will be of interest to us for meshing and measuring) is 0.2%. This difference is therefore negligible compared to the successive operations that have to be applied to the image.

IV.2.2. Region growing

The pixels corresponding to the noise are usually isolated pixels. Moreover, the surgical table constitutes a block of pixels which is detached from the bone system. To remove these pixels, the “region growing” technique is very useful. It does not consider a fixed threshold but identifies homogeneous regions around a starting point selected from the region of interest. By comparing the gradient similarity and the density value of the neighborhood, it enables to isolate completely the patient's bone. The result of this “region growing step” is shown in Figure 24.

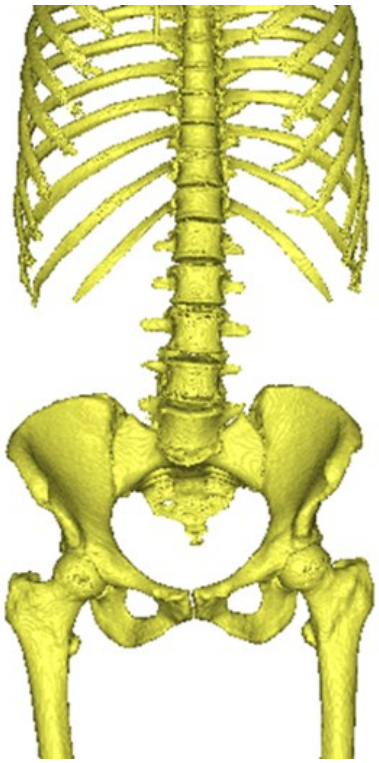

Figure 24. 3D scan of the patient after the “region growing” step on TAP scan.

As the scans correspond to the TAP region, the isolated object includes the bones of the thorax, spine, sacrum, femurs and pelvis. The pelvic bones must then be separated from the rest of the group.

IV.2.3. Split Mask

To separate the pelvis from the rest, the “split mask technique” enables the different regions of interest to be roughly marked on 5-6 sections and separated into several distinct masks. This technique uses the same principle as the region growing technique to delineate each region of interest. In this work, the complete TAP bone is separated into distinct parts: the vertebral column (green) with all the bones

of the upper body (thorax, sometimes shoulder), the sacrum (pink), the right femur (cyan), the left femur (orange), the right hemi-pelvis (blue) and the left hemi-pelvis (red). The two latter are the regions of interest to be saved (Figure 25). It should be noted that if the CT-scan image is of high quality, this separation can be done automatically. However, it is possible that despite all the precautions taken during the previous steps, one of the regions of interest nibbles on another through the joints that connect them. In this work, this defect is only observed in the sacroiliac joints.

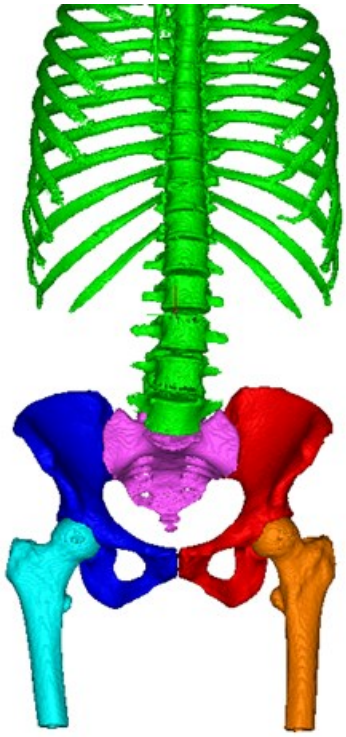

Figure 25. 3D visualization of the CT-scan after separation of the regions using the split mask tool.

IV.2.4. 3D Interpolation

The adjustment of the regions of interest requires the use of a semi-automatic “3D interpolate technique” so as not to have to retouch all the 2D sections of the 3D scan. It enables to correct only certain sections, to share regions of interest and then interpolate them over the entire structure. This technique is very useful for adjustments in the sacroiliac joints because they can easily be perceived as a homogeneous link between the iliac wings and the sacrum due to their close density. Once this step has been completed, the two sides of the patient's pelvis are finally obtained.

IV.2.5. Smart filling

After all these steps, “holes” may appear in the image of the pelvis (Figure 26). This is due to the quality of the CT-scan, but above all to the quality of the bone. In elderly patients with osteoporosis, the bone loses density. Certain regions therefore have a lower density on the Housfield scale and disappear during the thresholding step. These areas then need to be filled.

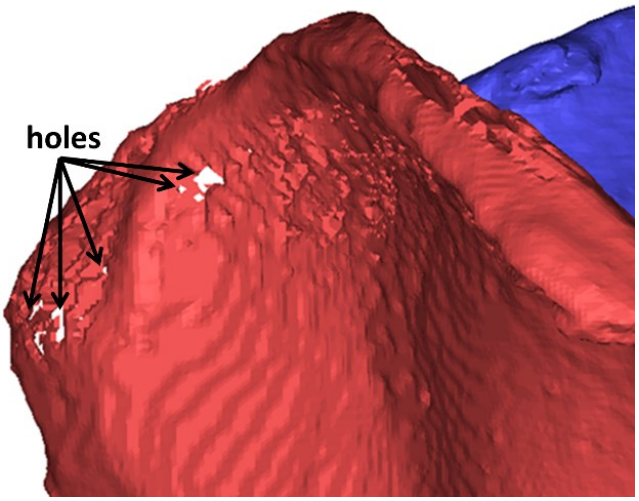

Figure 26. Appearance of “holes” on the iliac wing of the right hemi-pelvis.

The “smart fill” tool is a semi-automatic technique for finding the missing parts, either by designating the “hole closing distance voxel” function, which will be applied to the entire region automatically, or by filling the holes locally (Figure 27).

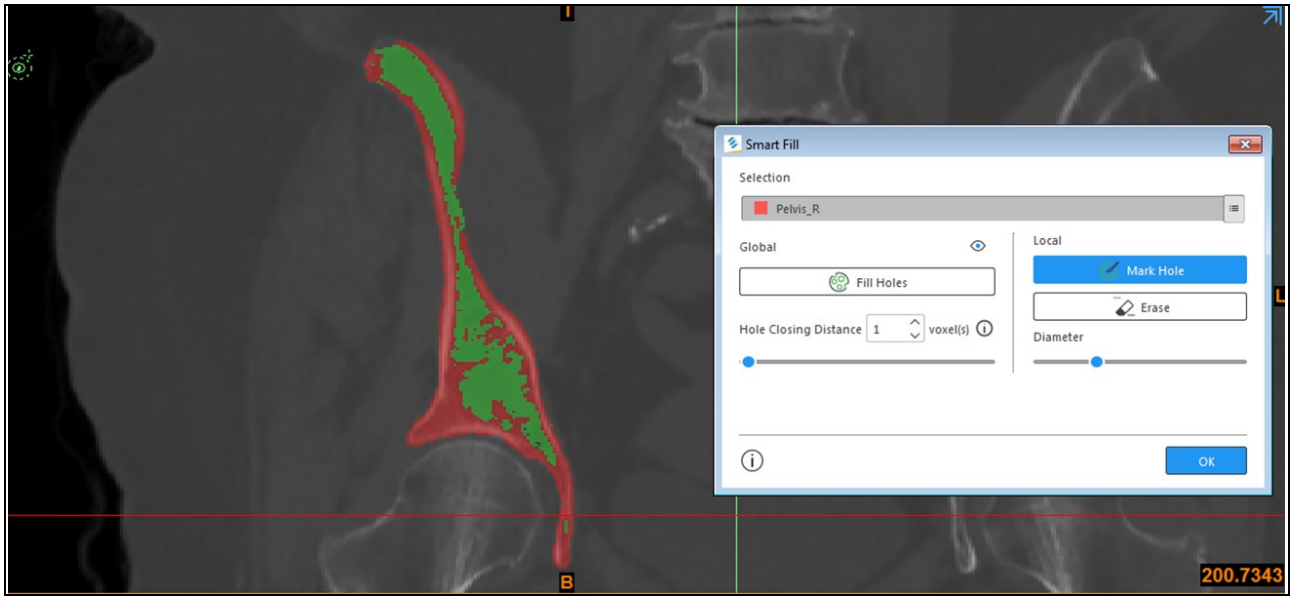

Figure 27. Filling of ‘holes’ on a sagittal section of the right pelvis.

Although this is the most tedious step, it also automatically interpolates the manual filling of holes, so that the operation does not need to be repeated on all 500 slices. The sagittal plane offers the best view for this type of procedure.

IV.2.6. 3D surface treatment

Once the two hemi-basins have been separated from the rest and processed, there are three further processing steps before the final image of the basin is obtained:

- Wrapping to fill in the remaining holes in 3D, to avoid errors in further analysis and measurements.

- Smoothing to smooth the pool by applying a low-pass filter to the voxels.

- Reducing the number of mesh triangles that covers the surface without changing its appearance.

These digital processes provide a better representation of the pelvis (Figure 28). After image segmentation has been completed, the first measurements concern the surface area and the volume of each hemi-pelvis, so that they can be compared.

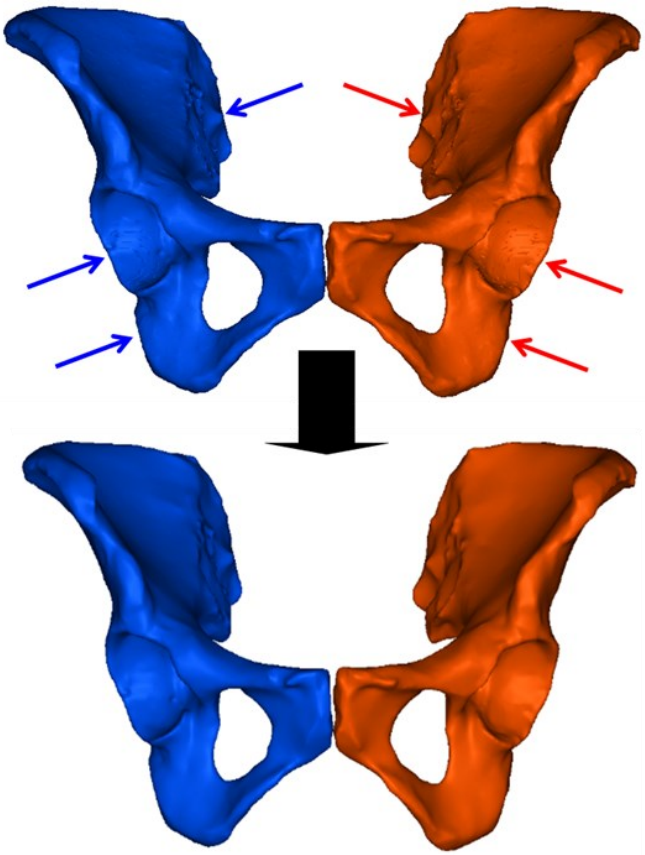

Figure 28. Pelvis before and after surface treatment.

IV.3. Data extraction with 3-Matic

For extraction of data with 3-Matic, this work focused on standardizing the mesh and obtaining a spherical shape for the acetabulum. The aim is to design with a suitable mesh so that the two hemi-pelvises can be compared, then to extract all the data required for the study in a format that can be read by Matlab.

IV.3.1. Standardization of the mesh

The mesh of each hemi-pelvis is processed in Mimics and the mesh size is adjusted (i.e. the choice of the triangle length that form the mesh) according to the complexity of the regions of interest in order to better represent the details (Figure 29). Hence the mesh size may be different between the two hemi-pelvises, leading to:

- an average difference of 5000 nodes between the two hemi-pelvises

- a different density of nodes in different regions of each hemi-pelvis

Consequently, the right and left hemi-pelvises display non-aligned nodes and a very heterogeneous anatomical positioning.

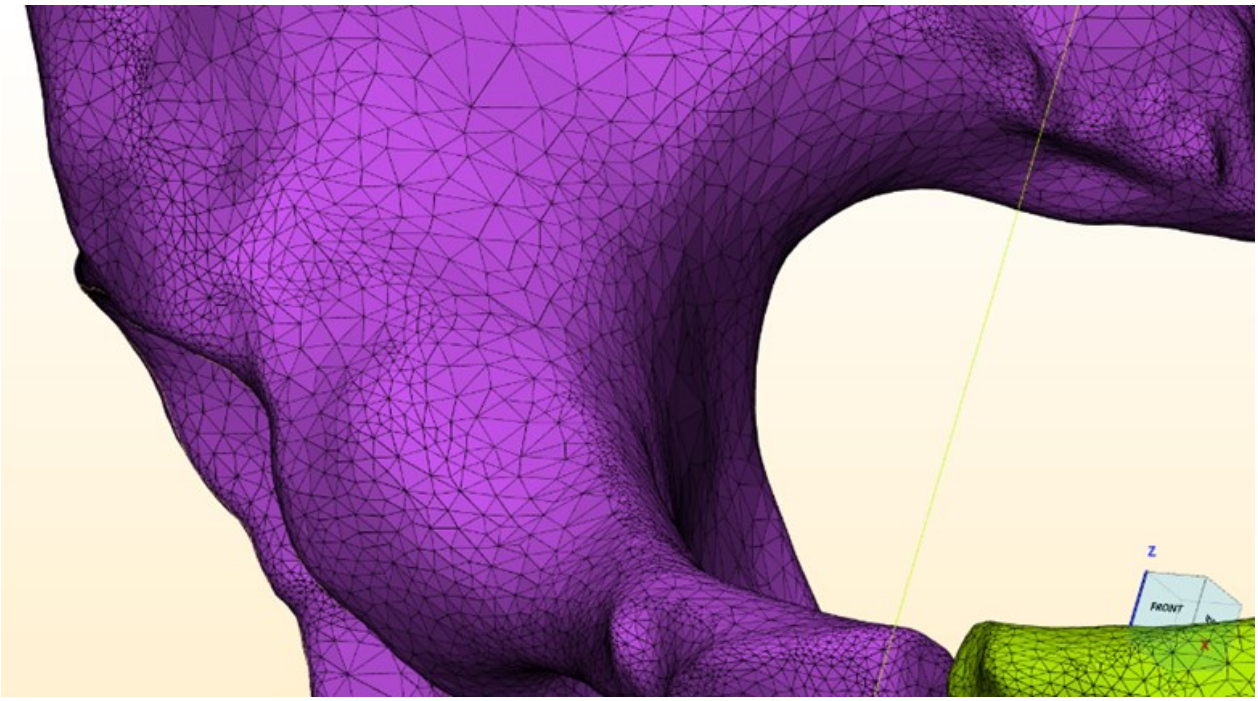

Figure 29. Initial mesh of the anterior column of the right hemi-pelvis.

As the study plans to carry out measurements and calculations between the two hemi-pelvises, it is necessary to standardize the mesh in order to eliminate these differences. The aim is to do not lose details in the regions of interest while not inflating the size of the data too much (~45,000 nodes per hemi-pelvis). Therefore, a side length of 1.3 mm is chosen for the triangles (Figure 30). This choice is also influenced by the memory required by the computer to carry out the remeshing, which increased exponentially as the length is reduced.

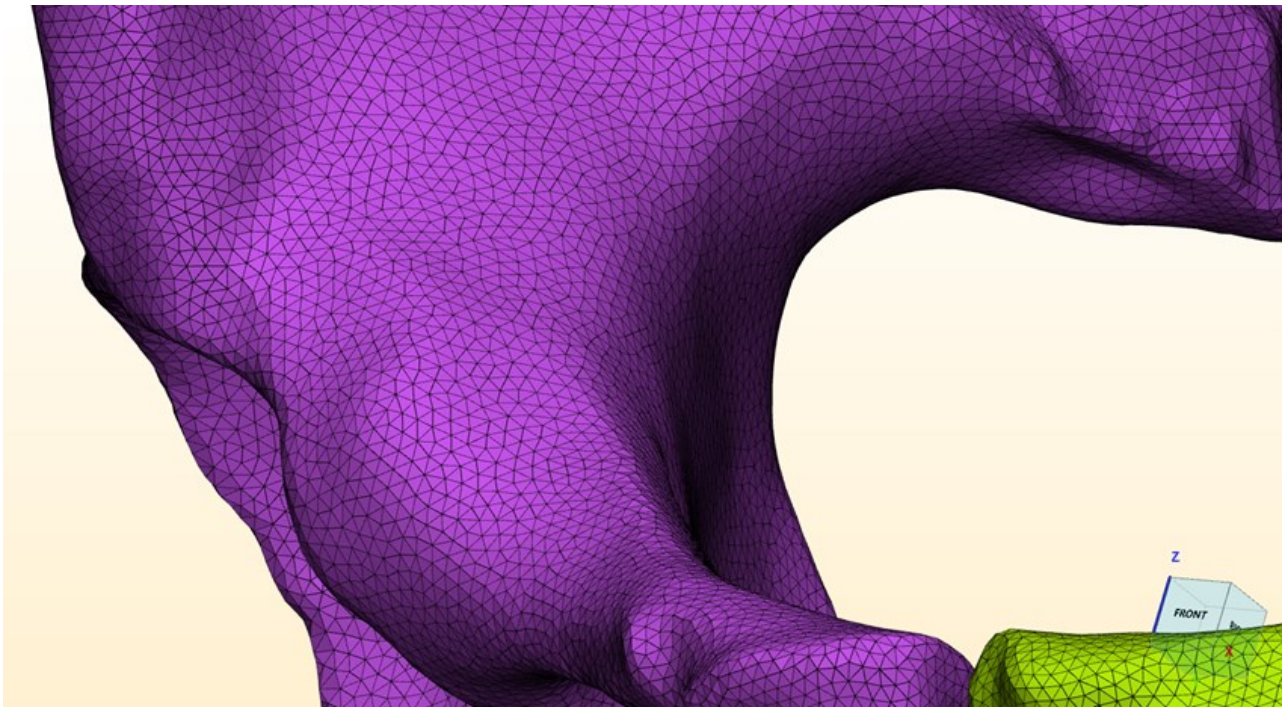

Figure 30. Uniform mesh of the anterior column of the right hemi-pelvis.

However, this step does not completely solve the problem of non-alignment of the nodes, that will be taken into consideration when comparing the two hemi-pelvises.

IV.3.2. Spherical shape of the acetabulum

In Total hip arthroplasty (THA), as described in section I.2.3.c (Figure 11), the acetabular part of the inserted prosthesis is shaped like a semi-sphere. To get an idea of the diameter of this semi-sphere and its position in the pelvis, some hospitals already use 2D measurement software such as MediCAD pre-operatively, for instance the Laveran Hospital in Marseille. However, this software may have

difficulty to model accurately complex fractures of the acetabulum, particularly those involving multiple fragments or significant displacement. In addition, as it is a 2D program, it is difficult to visualize the best approach for reduction. Planning is therefore based on the healthy contralateral hemi-pelvis.

Moreover, new visualization and 3D printing technologies enable orthopedic surgeons to train on the healthy hemi-pelvis. However, it must be noted that the 3D spherical shape of the fractured acetabulum before the injury can be different from the healthy side. As with the rest of the pelvis, we can first assume a similarity in the 3D spherical shape between the acetabular cavities on the two sides and measure the diameter of these semi-spheres for comparison. Therefore, 3-matic displays tools to create spheres inside the acetabulum of the pelvis.

After cutting the curve separating the surface of interest (the acetabulum) from the rest of the pelvis, the tool “Create Analytical Sphere” uses the least squares method between the center of the sphere and all the nodes on the surface to fit a sphere inside the acetabulum (Figure 31).

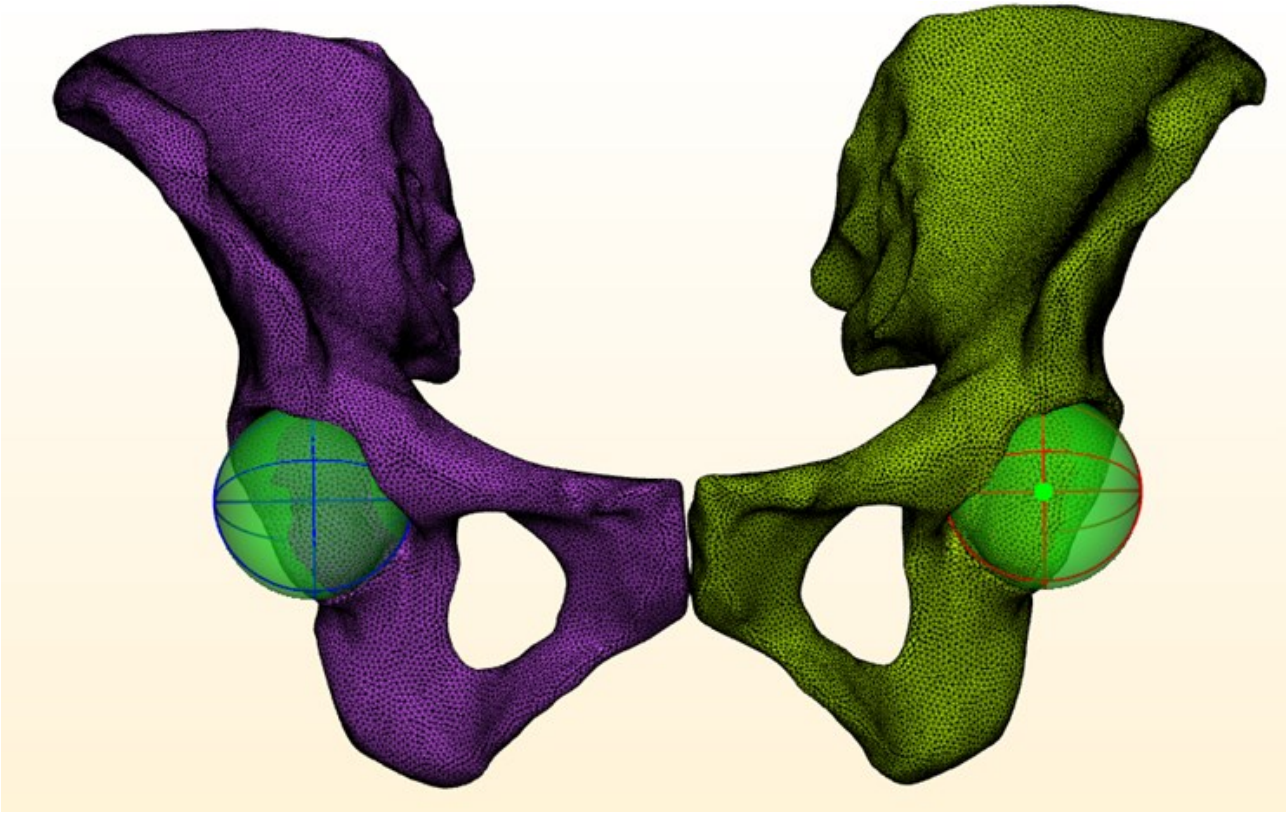

Figure 31. Sphere fitted in the acetabulum on 3-Matic.

IV.3.3 Data extraction

The previous steps enable to obtain two 3D hemi-pelvis with a suitable mesh so that they can be compared. Then, useful data must be extracted in visible format:

- the coordinates of the nodes in the reference frame of the software, which is the one existing by default;

- the links between the nodes that form the sides of the triangles covering the surface of the hemi-pelvis;

- the curvature at each point, which will be very useful for finding the anatomical landmarks in 3D, on the scanner that the orthopedic surgeon sees on the 2D slices.

All of this data is exported in .txt format. There are two different types of files:

- a file containing the coordinates of the nodes in the same order as in the 3D reference of the software.
- a file containing the trio of nodes forming the triangles and the curvature value for each node.

The algorithm developed in this work used five steps

- **Step 1:** Creating manually a plane of symmetry by selecting the anterior-superior iliac spines, which are the anterior ends of the iliac crest, as characteristic nodes. The aim is to create a mid-plane between the two nodes.
- **Step 2:** Duplicating a mirror image of each side of the pelvis in relation with this plane. The result is 4 hemi-pelvises: 2 left, 2 right.
- **Step 3:** Alignment by “Global registration” of the mirror images with their contralateral sides (e.g. mirror image of the right hemi-pelvis with the left hemi-pelvis).
- **Step 4:** Analysis of the curvature of the original hemi-pelvis and comparative analysis of the mirror images with their contralateral sides.

In conclusion, the table 8 summarizes all the steps for 3D segmentation of CT scan images and data extraction developed in this work of Master Thesis. The evaluation of accuracy is alo presented.

Methods	Steps and parameters
3D CT scanner	Values of tissue absorption, converted into Hounsfield units (HU) Three-dimensional visualization of anatomical structures in regular sections Accuracy: 0.6 to 1 mm
Image segmentation on Mimics	Thresholding Region growing technique Split mask 3D interpolation Smart fill tool Mesh processing
Data extraction on 3-Matic	Uniform mesh size: 1.3 mm Fit of spheres in the acetabulum Data export (points, mesh and curvature values)

Table 8. Steps and parameters for 3D segmentation of CT scan images and data extraction.

IV.4. Matlab algorithms to evaluate the symmetry

After extraction of data, Matlab algorithms are used to define the plane of symmetry, to align and to quantify the symmetry between the two hemi-pelvises.

IV.4.1. Plane of symmetry

There are two ways of defining the plane of symmetry:

1) The degree of resemblance between one hemipelvis and the mirror image of the other hemipelvis can be defined by calculating the deviation between the two surfaces, as studied by Eat et al.[21] and Zheng et al.[22]

2) The symmetry can be studied from a mathematical point of view, i.e. in relation to a point or plane of symmetry. As the human body is anatomically symmetrical with respect to the sagittal plane, this plane is used to study the symmetry between the two hemi-pelvises.

Thus, this work focuses on the two definitions of the plane of symmetry, and the link between them, for a better understanding of this symmetry. The aim is to be able to use it effectively in new methods of assisting surgery.

a) Mirror image with regard to the plane of symmetry (MIPS)

The mathematical point of view of the symmetry corresponds to the evaluation of the mirror image with regard to the plane of symmetry (MIPS), with the following two steps:

- **Step 1:** Search for the midpoints of the pairs of nodes belonging to the two half-pelvises, that are approximately aligned according to 3-Matic, in order to fit a first imperfect symmetry plane.
- **Step 2:** The mirror image of each half-pelvis is generated from this plane of symmetry.

The plane is therefore generated on Matlab, after extracting the nodes and links from the mesh on 3-matic. The idea being to consider all the geometric aspects of the basin, the ideal would be to form the plane by the midpoints of each pair of nodes aligned between the two surfaces. However, as it is seen above, the meshes are not the same in each hemi-pelvis, which results in different numbers of nodes and little alignment.

b) Adding rigid alignment to MIPS method

In this work, to avoid the problem of non-alignment, a rigid alignment between the mirror image and its original equivalent is added to MIPS. Therefore, this work implemented a process using four steps to the two steps of MIPS:

- **Step 1:** Search for the midpoints of the pairs of nodes belonging to the two half-pelvises, that are approximately aligned according to 3-Matic, in order to fit a first imperfect symmetry plane.
- **Step 2:** The mirror image of each half-pelvis is generated from this plane of symmetry.
- **Step 3:** A rigid alignment is made between each hemi-pelvis and the mirror image of its contralateral.
- **Step 4:** The first step is repeated between each hemipelvis and its mirror image after alignment. It must be pointed out that the mirror image has the advantage of having the same number of nodes and perfect alignment with its original.

- **Step 5:** An average plane of the two planes matching with the previous step is generated, giving the desired plane of symmetry.
- **Step 6:** Steps 2 and 3 are repeated, but this time with the final symmetry plane, and the transformation matrices on both sides are saved.

As the 3-matic software does not contain the necessary tools to find the best plane of symmetry between a hemi-pelvis and his contralateral, an algorithm is developed in this work to carry out all these steps. The function used for the alignment is an algorithm based on Coherent Point Drift (CPD) registration. This is a robust probabilistic algorithm for registering multidimensional point sets for rigid and non-rigid transformations. The general methodology was presented by Myronenko et al.[58]

The algorithm used for MIPS plus rigid alignment is presented in Appendix 2 and it produces the following outputs:

- the first imperfect plane generated in the first step of the algorithm,
- the final plane from which symmetry will be studied,
- the new system generated by this sagittal plane and the frontal and transverse planes, adding the most distant points on the Y and X axes,
- the two transformation matrices for each hemi-pelvis (l = left and r = right).

Once the plane and the transformation matrices are determined, the analysis of symmetry by evaluation of the deviation between the two hemi-pelvises is carried out.

IV.4.2. Measuring deviation

The measurement of the deflection between surfaces is first inspired by previous studies:[21-23] For instance, Zhang et al.[23] defined the 3D deviation for a point y in a model Y to the equivalent point x in the model X (e.g. the two hemi-pelvises) as:

$$d(y,x) = \min_{x \in X} ||y - x||_2 \quad (2)$$

With $||.||_2$ the Euclidean norm.

Thus, the mean deviation of the entire model Y from the model X is calculated using the root mean square (RMS) value:

$$RMS(X,Y) = \sqrt{\frac{1}{n+k}\left[\sum_{i=1}^{n} d^2(x_i,Y) + \sum_{j=1}^{k} d^2(y_j,X)\right]} \qquad (3)$$

However, this formula gives a result that is far too large and non-consistent with reality. This is due to different meshes on the two hemi-pelvises, and therefore on the mirror image of a hemi-pelvis compared to its healthy contralateral hemi-pelvis. As the arrangement of the nodes is not the same when the two surfaces are stuck together, there may be some deviation when comparing the nodes, as shown in the diagram below (Figure 32). In figure 29, y_1 belongs to Y and x_1 is the closest point to y belonging to X. Even when the top surfaces of X and Y are aligned (i.e. at 0mm deviation), there is a non-zero distance d between y_1 and x_1.

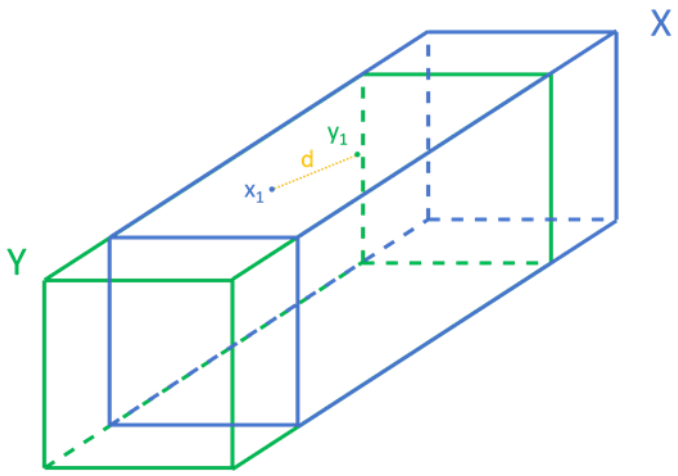

Figure 32. Diagram of the deviation problem related to two different meshes.

Hence, the formula therefore is rearranged in this work considering the limitation described above. It seems that a better way to define distance is that of a point y on model Y with its projection onto model X. As the surfaces of the models are made up of triangles, the idea is to project y onto the triangle of X, closest to y using the following formula:

$$d'(y,X) = \left|\left|y - y_{pro}\right|\right|_2 \qquad (4)$$

With $||.||_2$ the Euclidean norm and y_{pro} the projection of y on the plane formed by the nearest triangle in the surface of X (figure 33).

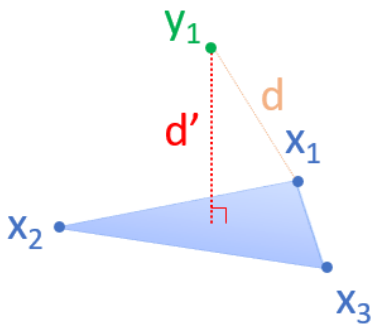

Figure 33. Diagram of the deviation considering the projection.

Furthermore, the deviation can be measured between one of the hemi-pelvises and the mirror image of its contralateral, as it was done by Ead et al.[53] and Zhen et al.[54] However, the alignment algorithm may not give the same result on both sides and we are interested in left-right symmetry as well as right-left symmetry. It is therefore considered more relevant to measure this deviation for both sides according to the following final formula:

$$RMS(X,Y) = \sqrt{\frac{1}{n+k}\left[\sum_{i=1}^{n} d'^2(x_i', Y) + \sum_{j=1}^{k} d'^2(y_j', X)\right]} \quad (5)$$

With X the right hemi-pelvis right, Y the left hemi-pelvis left, X' the mirror image of the right hemi-pelvis right and Y' the mirror image of the left hemi-pelvis.

In this work, a deviation function (appendix 2) has been developed to measure d. It takes as input two sets of nodes, with their link forming the mesh. To calculate the deviation of one point from the other, the final formula (5) is used. In other words, this algorithm compares the distance of one surface from another by following four steps:

- **Step 1:** for each node i of hemi-pelvis, its v nearest neighbors of hemi-pelvis 2 are determined.
- **Step 2:** the mesh triangle of hemi-pelvis 2 closest to i, formed by three nodes among the v neighbors, is determined.
- **Step 3:** point i is projected onto the plane formed by the triangle. Then, the distance between i and i_{pro} is calculated.
- **Step 4:** point i is classified according to its absolute distance from hemi-pelvis 2, using a threshold based on criteria defined by the orthopedic surgeons. This enables local symmetries and asymmetries to be visualized. In this work, the threshold value is that of Matta's criterion, i.e. 2mm.

The results of interest are:

- the rates of deviation below 2mm
- RMS of deviations
- the standard deviation of deviations
- the vector of all distances calculated

The value of the vector assigned to each node is:

- 0 for nodes displaying no triangle despite the 6 neighbors that are considered. These nodes represent 0.005% of the nodes and therefore have only a minimal impact on the analysis.
- 1 for nodes with a deviation of less than 2 mm (permissible deviation)
- 2 for nodes with a deviation of more than 2 mm (asymmetry)

This value provides a clear view of the symmetrical or non-symmetrical regions of the pelvis (Figure 34).

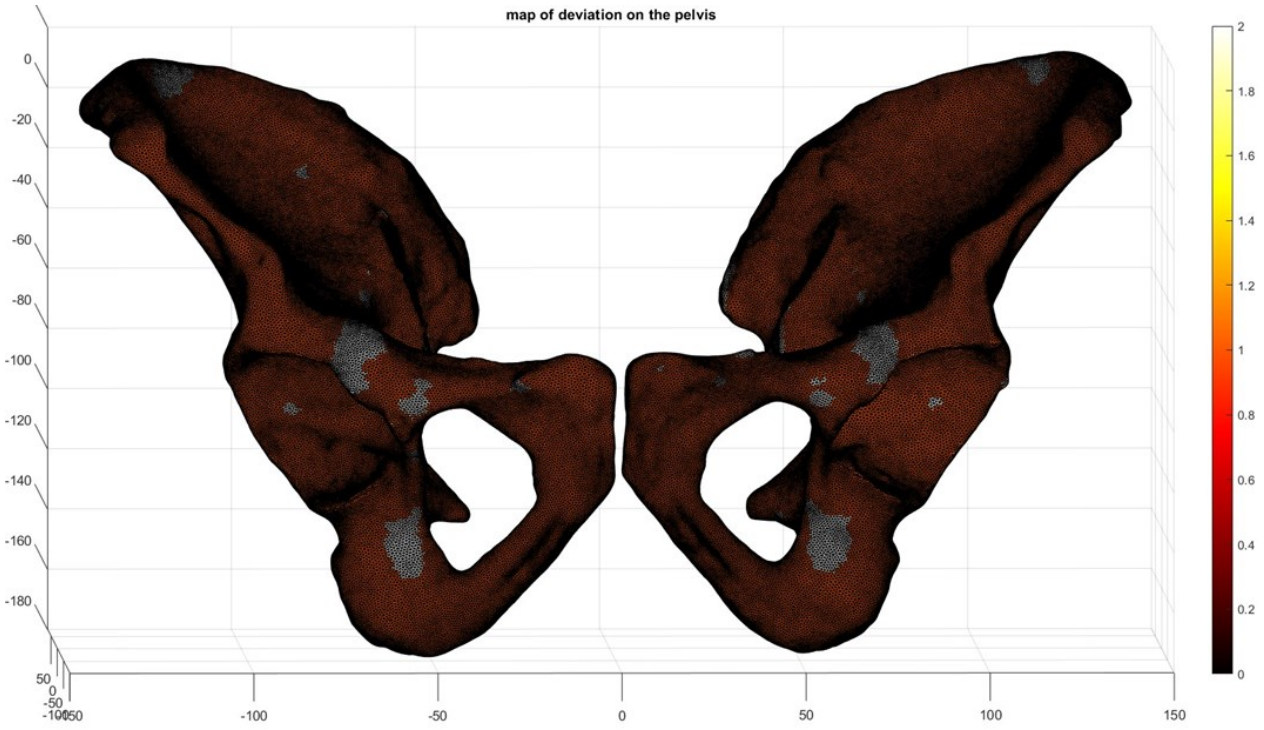

Figure 34. Analysis of symmetric (orange) and asymmetric (white) regions of the pelvis. Nodes that are not considered (black) are also represented.

Measurements are proceeded on all 28 patients, for each hemi-pelvis with the mirror image of its contralateral. Deviations are assessed according to the plane of symmetry only, and according to the plane of symmetry plus the rigid alignment. All the measurements carried out during the Master thesis work are summarized in table 9.

Softwares	Measurements on each hemi-pelvis
Mimics	Surface in $\times 10^4$ mm^2 Volume in $\times 10^4$ mm^3
3-Matic	Diameter of fitted spheres in the acetabulum in mm
Matlab	Percentage of permissible deviations (< 2 mm) } MIPS RMS of the deviation in mm Percentage of permissible deviations (< 2 mm) } MIPS + rigid alignment RMS of the deviation in mm Norm of difference in translation in the rigid alignment between left and right side in mm

Table 9. Summary of measurements carried out on 28 patients.

V. Results and discussion

The comprehension of pelvic symmetry is refined using the mirror image with regard to the plane of symmetry (MIPS) method with and without rigid alignment and evaluated on CT-scanner image of 28 patients. Then, the influence of age and sex is analyzed for symmetry, but also on global data obtained on the pelvis. Finally, the results are compared to the literature.

V.1. Study of symmetry

V.1.1. Volume, surface and diameter of the acetabulum

First, the symmetry of the pelvis is evaluated through the difference (in percentage) of the volume, the surface and the diameter of the acetabulum between the left and right hemi-pelvises for each patient. A t-test Student is applied in order to conclude on the relevance of the difference (table 11). There is no statistically difference in volume (p = 0.98), in surface (p=0.99) and in diameter for the acetabulum (p = 0.73).

	Difference (%)	p_{value}
Surface	1.03 ± 0.81	0.99
Volume	1.80 ± 1.29	0.98
Diameter of acetabulum	0.35 ± 0.29	0.73

Table 11. Percentage difference between left and right side of the pelvis with p_{value} of t-test Student.

V.1.2. Comparison between MIPS and MIPS plus rigid alignment methods

The MIPS method is applied either solely from a mathematical point of view, or from a geometric point of view by adding a rigid alignment between the mirror image and its original equivalent. The steps of the algorithm are described in part III.4.1. For each method, the percentage of deviations within ± 2-mm and the RMS are measured. The mean values with standard deviation (SD) of each measure is regrouped in the table 12.

	MIPS	MIPS + rigid alignment
Average percentage of deviations within ± 2-mm	66.69 ± 16.47%	91.49 ± 3.71%
Average RMS	2.18 ± 0.83 mm	1.16 ± 0.18 mm
Average difference in translation induced by rigid alignment		1.68 ± 1.41 mm

Table 12. Comparison between left and right hemi-pelvises with their respective mirror images, using the plane of symmetry (MIPS) method applied with or without rigid alignment.

In table 12, the symmetry studied in each lead to the following conclusions:

- With the MIPS method, the pelvis does not appear to be symmetrical enough for the surgeon because the average RMS of 2.18 ± 0.83 mm is higher that the admissible deviation of ±2mm.
- Adding the rigid alignment to MIPS method leads to small RMS values and high percentage of points within the ± 2-mm range for all 28 patients. These results are close to those found by Ead et al.[53], and shows that the pelvis is symmetric and
- Concerning the average difference in translation induced by the rigid alignment algorithm (1.68 ± 1.41 mm), the best symmetry plan found in MIPS method seems not sufficient to obtain the same result as after alignment. Consequently, the use of geometric symmetry as an aid to surgery have to be used carefully, as alignment is not carried out in the same way on both sides. This is crucial in surgery as the accuracy is expected to be of the order of a millimeter. Consequently, a shift of just a few millimeters can induce to an unbalanced distribution of loads on the pelvis, leading to coxarthrosis in the cartilage of the acetabulum that is most heavily loaded.

V.2. Statistical analysis on the influence of age and sex

V.2.1. Summary of patient samples

In this work, CT-scans of 32 subjects are collected, but 4 of them have unusable data (poor resolution, segmentation too tedious, etc.). The average age is 55.4±20.1 years old with a range of 22-84 years old. It must be noted that the series is split equally between men and women (14 of each) so that the results can be compared not only by age but also by sex.

The 28 patients selected are separated in four samples according to age and sex, as shown in table 10.

Age	Men	Women	Total
≤ 60 years old	**5**	**9**	**14**
> 60 years old	**9**	**5**	**14**
Total	**14**	**14**	**28**

Table 10. Samples for statistical analyses.

V.2.2. Influence of age and sex on the symmetry of pelvis

The samples for age and sex analysis are of reasonable size (n=14). Hence, the normality test of Shapiro-Wilk is applied to each of them for each variable. It must be pointed out that the majority of the results rejected the null hypothesis. In addition, the samples combined (young men, young women, old men, old women) are too small to compare them using a parametric test. Consequently, to compare the symmetry in the different samples, it is more appropriate to use a non-parametric test instead of t-student test. As the samples are unpaired, the test chosen is the Wilcoxon rank sum test (ranksum() on Matlab) which is equivalent to the Mann-Whitney U-test. Level of significance is set at $p < 0.05$. RMS and deviations obtained with MIPS with and without rigid alignment are presented in table 13.

	Men versus Women	**Young versus Old**	**Young men versus Old men**	**Young women versus Old women**	**Old men versus old women**	**Young men versus Young women**
Deviation plane	0,1129	0,7304	0,7972	1,0000	0,0120	0,6064
Deviation plane + alignement	0,6961	**0,0258**	**0,0420**	0,3636	0,7972	0,7972
RMS plane	0,1904	0,8362	0,8981	1,0000	0,0829	0,6064
RMS plane + alignment	0,3573	**0,0081**	**0,0230**	0,2398	0,4186	1,0000
Difference in the translation	0,2905	0,5051	0,8222	0,8981	0,4376	0,7972
Difference in the diameter of the acetabulum	0,4763	0,5052	0,1768	0,6993	0,3636	0,9710
Difference in the surface area of the pelvis	0,4763	0,1354	0,7972	0,6993	0,3636	0,5185
Difference in the volume of the pelvis	0,1478	0,9817	0,8981	0,6064	0,2977	0,3636

Table 13. p_{value} of Mann-Whitney test for comparison between right and left half-pelvis.

The p_{value} shows obvious differences (smallest p_{value} in blue in table 12) for the deviation plane plus alignment and RMS plane plus alignment, in the samples comparing young and old patients and young and old men. However, it is not observed in the sample comparing young and old women.

This study shows difference with age and sex only for the symmetry calculated geometrically with MIPS plus rigid aligment method. The p_{value} shows obvious differences (smallest p_{value} in blue in table 13) for the deviation plane plus alignment and RMS plane plus alignment, in the samples comparing young and old patients and young and old men. However, it is not observed in the sample comparing young and old women. So, it seems that there is an influence of age, more specifically in the case of men, as shown by the trend line in Figure 35.

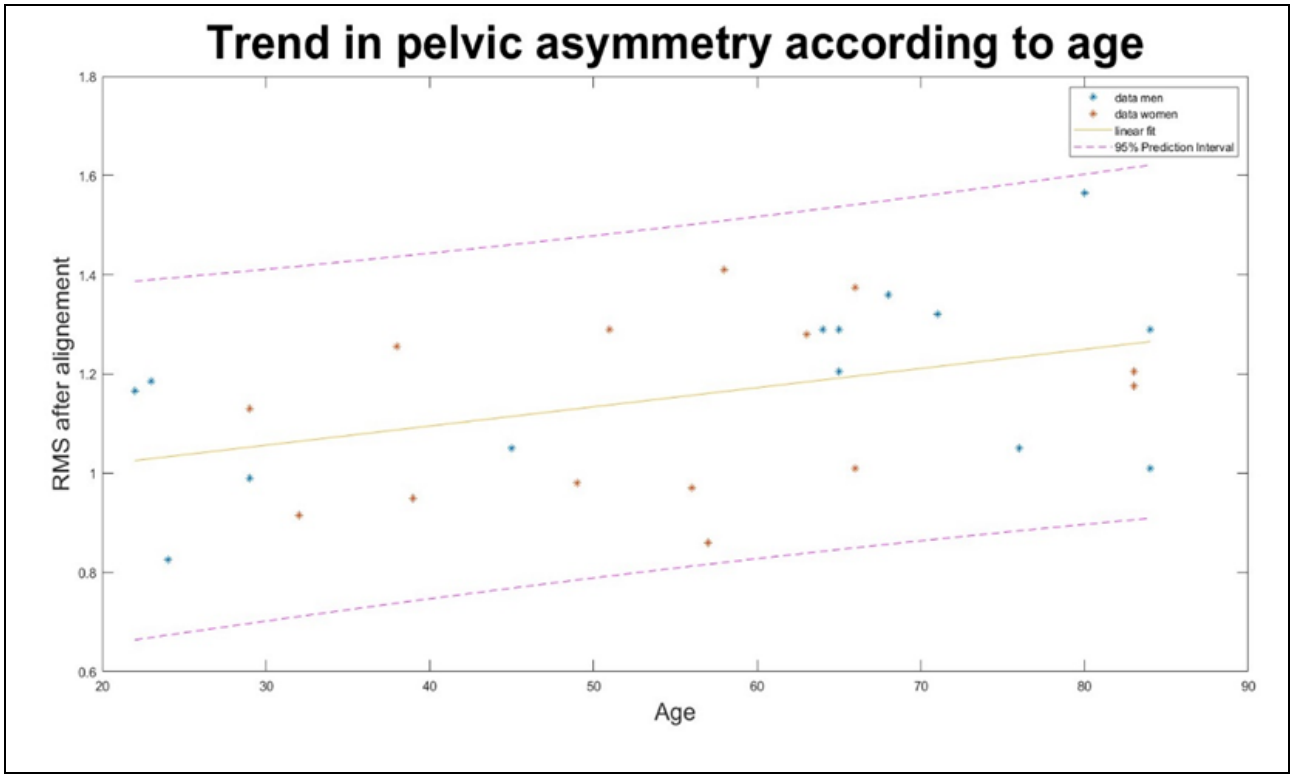

Figure 35. Trend in pelvic asymmetry through the RMS of distances according to age and sex.

The difference related to age and sex can be explained by differences in loading during the lifetime for men compared to women, and/or hormonal differences between men and women. However, as this is the first study to find an influence of age, it would be appropriate to repeat the analysis on larger samples and to have more information about patients, such as their hormonal changes (due to the menopause, for example) and their activities or jobs (which involve repeated effort, for example).

V.2.3. Influence on the pelvis volume, surface area and the acetabulum diameter

The mean value of pelvis volume, its surface area and the acetabulum diameter are measured (Appendice C), and Mann-Withney test is applied between each sample (Table 14).

	Men versus Women	Young versus Old	Young men versus Old men	Young women versus Old women	Old men versus old women	Young men versus Young women
Mean volume of pelvis	**0,0004**	0,1611	0,7972	0,6064	**0,0290**	**0,0070**
Mean surface of pelvis	**0,0003**	0,0695	0,2398	0,3636	**0,0290**	**0,0010**
Mean diameter of acetabulum	**0,0001**	0,3952	0,5005	0,7972	**0,0120**	**0,0010**

Table 14. p_{value} of Mann-Whitney test for global pelvis data.

A clear difference according to sex, whatever their age is observed on all the data, supported by statistical tests. These differences are illustrated in Figure 36 for the mean pelvis volume, in Figure 37 for mean pelvis surface area and in Figure 39 for the diameter of the acetabulum.

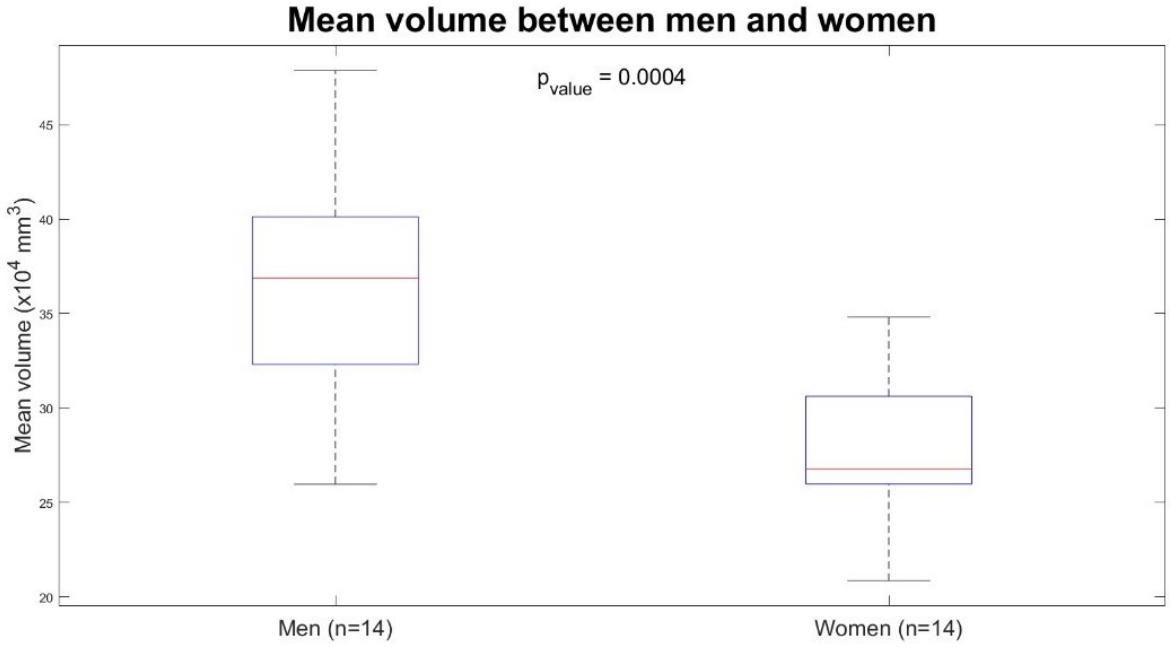

Figure 36. Boxplot with p_{value} of Mann-Whitney test for mean pelvis volume between men and women.

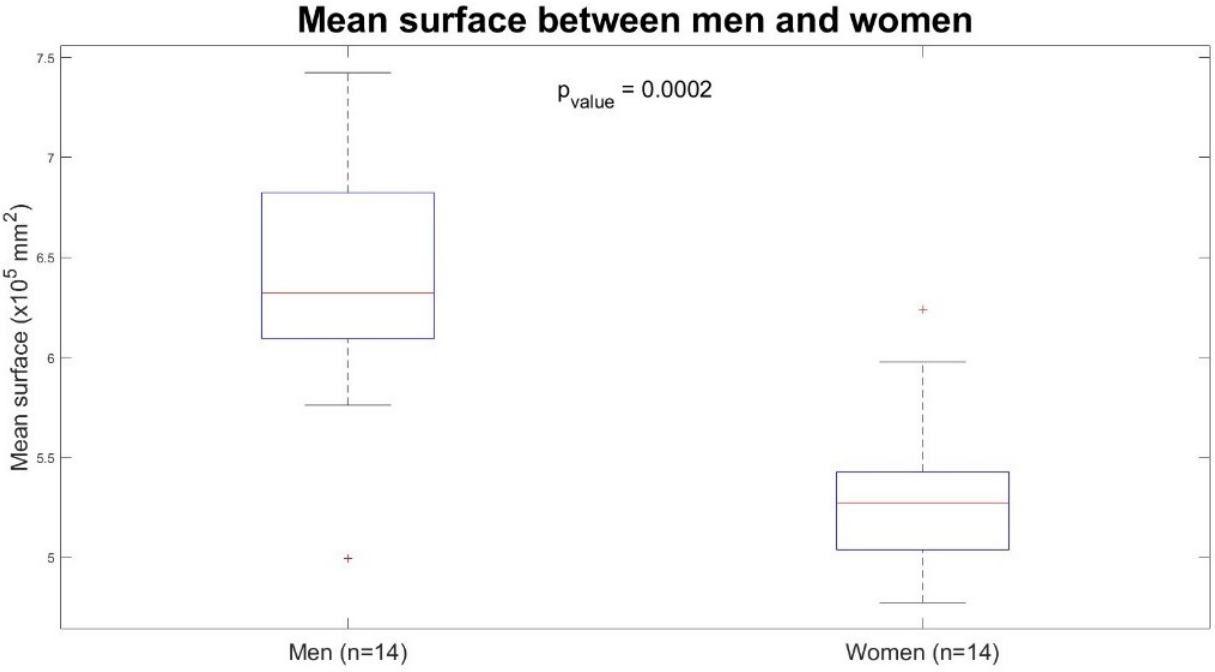

Figure 37. Boxplot with p_{value} of Mann-Whitney test for mean pelvis surface between men and women

Figure 38. Boxplot with p_{value} of Mann-Whitney test for mean diameter of acetabulum between men and women

V.3. Comparison with literature

V.3.1. Limitations of studies in the literature

In the literature, studies on pelvic symmetry used mainly methods based on anatomical landmarks or pre-formed implants.[58,59] For example, Boulay et al. analyzed 71 pelvic anatomical variables to assess symmetry between the left and right hemi-pelvises of 12 patients.[58] They found symmetry in 6 patients. Osterhoff et al. confirmed the symmetry of the peri-acetabular surface by comparing the differences between the hemi-pelvis and a virtual reference implant.[59]

Although these studies are significant, they did not consider the irregular geometric shape of the pelvis. As a result, there is considerable intra- and inter-observer variability. To avoid these limitations, pelvic symmetry should be assessed by examining the entire 3D geometric shape without using specific landmarks. To our knowledge, only a few studies have begun to examine the complex geometric shape of the pelvis.[52,57,60]

V.3.2. Contribution of the master thesis work

The work carried out in this master thesis complements the initial studies in the literature. In particular, comprehension of pelvic symmetry is refined, investigating two points of view:

- Mathematical, with the distance of points from the 'best' sagittal plane between the two hemi-pelvi
- Geometric, after alignment of a hemi-pelvis with the other.

In this context, the volume and surface area of the pelvis are calculated. In addition, the diameter of the spherical shape of the acetabulum is accurately measured, as this is essential for Total hip arthroplasty. This measurement can be semi-automated, because once the 3D reconstruction has been carried out, the measurement of global symmetry is fully automated in Matlab. In addition, Matlab programming enables local measurements to be made semi-automatically. Only the coordinates of the start and end points of the curves need to be entered before the algorithm is launched.

This work shows that the pelvis is not mathematically symmetrical. However, it is symmetrical in the geometric point of view after alignment, which involves defining a transformation matrix to align the mirror of one of the hemi-pelvises with its contralateral. This enables to demonstrate that the difference in translation between the alignment of the right hemi-pelvis and that of the left hemipelvis is not negligible.

VI. CONCLUSION

This master thesis uses CT images to analyze the symmetry between the two sides of the bony pelvis of healthy patients. CT scan images of pelvises are collected from a cohort of 28 patients. As the images are in 2D, the first requirement is to obtain a 3D visualization of the pelvis Then, modelling tools are used to compare global and local symmetries between both hemi-pelvises: 3D segmentation with the software Mimics, data extraction with 3-Matic and symmetry calculation with Matlab.

The pelvic symmetry is evaluated with the method using the mirror image with regard to the plane of symmetry (MIPS method), with and without rigid alignment. Then, pelvic symmetry, as well as the general shape of the pelvis and the influence of age and sex are analyzed. The right and left hemi-pelvises are shown to exhibit a high degree of symmetry in geometric point of view, but not in mathematical one. The calculation methods used in this work for measuring the pelvic symmetry are presented and justified. Thus, this work fills in the gaps left by previous studies in the literature.

The results concerning symmetry is very useful in new technologies to aid surgery, such as 3D modelling software (for example Mimics, which is used in this work) and 3D printing. Orthopedic surgeons can thus confirm the effectiveness of using the mirror method in the planning process. Furthermore, a better understanding of symmetry at the local level, as well as the influence of factors such as gender, childbirth, activities and physical work, enable even more patient-specific planning and fixation plate for the surgeon. The aim is to reduce the alarmingly high mortality and morbidity rates associated with pelvic fractures, by reducing the length of surgical treatment and waiting times.

The perspectives of this work concern the responses to be provided in the future to the limitations that need to be considered:

- The CT-scan images correspond to 2D slices of the pelvis, whereas it has a complex 3D shape. Hence, the thickness of the slices varies from one patient to another, depending on the manipulator. The thickness varies between 0.6mm and 1mm, which has an impact on the resolution of the 3D visualization obtained during the segmentation-reconstruction phase.

- As the segmentation phase is not fully automated, there is always some uncertainty due to the operator. Although it is not possible to quantify the error generated by all the processing steps, another study of 3D reconstruction of CT images of the tibia carried out by Van den Broeck et al. estimated an average error of 0.55 mm.[59]

- The areas imaged by CT-scan include the anterior wall of the acetabulum, the posterior wall of the acetabulum, the ilioischial line, the obturator frame and the superior column. It must be pointed out that the roof of the acetabulum is not considered, as 3D visualization shows that it is encompassed by the anterior and posterior walls. This is also the case for the radiographic U, which is not distinctive in 3D.

- The sample of 5 to 9 patients per criteria is too small for reliable statistical tests on age and sex at the same time. In addition, having more information on the patients would make it possible to study the influence of social characteristics such as the type of work or biological characteristics such as childbirth.

VII. PERSPECTIVES

This Master thesis is followed by a Doctoral thesis entitled ‘Development of a digital twin for the functional optimization of pelvic fracture treatment at the Institut des Sciences du Mouvement (ISM) d'Aix Marseille Université (France).

The aim is to achieve automated, personalized pre-operative planning through the development of a digital twin of the fractured pelvis. In other words, a virtual model that faithfully reflects the patient's fractured pelvis. Thanks to this, simulations can be carried out before the operation to optimize management of the fracture. In this context, the surgeon's problem is to know how to get the bone to rebuild itself healthily, in other words how to return the pelvis to its initial state (before the fracture). Ideally, images of the pelvis before the fracture would be available, but this is never the case. To fill this information gap on the initial state of the pelvis, the idea is to refer to the healthy side and manipulate its mirror image to compare it with the fractured side. This master thesis provides information on pelvic symmetry for the AI implementation that will enable this reconstruction.

In order to identify the regions of interest and take measurements, an anatomical reference point that can be replicated and generated automatically, whatever the patient and the manipulator, has to be defined. The sagittal plane of symmetry generated during this master thesis will form the first axis of this reference frame, which will be completed by two characteristic points of the pelvis. As the creation of this reference frame will have to be feasible on a fractured pelvis as well as on a healthy one, the choice of these two points will be constrained.

In a second stage, the digital twin will be optimized to be used with standardized implantable devices. Therefore, a mechanical analysis of the pelvis will be carried out virtually in order to approximate its properties. The repair method can then be validated by experiments on Sawbones or cadaveric pelvis models. Ideally, the fracture environment would then be added, i.e. the soft tissues surrounding the site, to provide the surgeon with the most realistic conditions. This additional input could guide the choice of approach during the surgery and cause the least damage.

Consequently, the aim of the Doctoral work is to be able to plan the surgical procedure in silico. The digital twin will be not only used in traumatology, but also for educational purposes, to train young orthopedic surgeons.

Appendix A: function perfect_plane.m

```
%% Perfect plane
% Gives the percentage of points below a deviation threshold as well as
% the mean distance (RMS) and standard deviation of this deviation
% To perform this analysis, for each point on one of the objects,
% we look for the triangle formed by the nearest neighbours of the point of interest
% on the mesh of the other object, and then calculate the deviation between
% the point of interest and its projection on this triangle.

% Input :
% P_r : matrice nx3 containing a set of points which are the nodes of
% one of the two hemi-pelvis
% P_l : matrice nx3 containing a set of points which are the nodes of
% the mirror of P (after or before the alignement step)
% Nodes of P_r and P_l are approximately aligned
% data_r : matrice nx3 containing a set of points which are the nodes of
% one of the two hemi-pelvis
% data_l : matrice nx3 containing a set of points which are the nodes of
% the mirror of P (after or before the alignement step)

% Output :
% plane_final : vector 1x4 with the coefficient a, b, c, d of the equation of
% the plane of symetry generated by the algorithm
% plane : vector 1x4 with the coefficient a, b, c, d of the equation of
% the first plane "imperfect" between the two hemi-pelvis
% system : new system generated from the symetry plane (saggital plane) and
% the frontal and tranverse planes
% Transform_r and Transform_l : structure of the estimated transformation parameters:
%
%           .Y     registered Y point-set
%           .iter  total number of iterations
%
%           .R     Rotation/affine matrix.
%           .t     Translation vector.
%           .s     Scaling constant.

% Transform_r : for aligning the left-side mirror image,
% relative to the plane_final, with the original right-hand side
% Transform_l : for aligning the right-side mirror image,
% relative to the plane_final, with the original left-hand side
```

```
function [plane_final, plane, system, Transform_r, Transform_l]= perfect_plane(P_r, P_l, data_r, data_l)
    % Establish a first "imperfect" plane of symmetry from the two original semi-pelvis
    % by fitting it to the midpoints of the pairs of aligned points.
    [n,d,~,~]= find_plane_basic(P_r,P_l,1);
    plane = [n',d];

    % Generate mirror of each semi-pelvis along the "imperfect" plane
    data_l_mirror =  mirror(data_l,plane);
    data_r_mirror =  mirror(data_r,plane);
    % Align the mirror image of the left-side semi-pelvis with the original
    % on the right side
    [X_r,Y_l,~] = align_nonrigid(data_r,data_l_mirror,"rigid");
    % Align the mirror image of the right-side semi-pelvis with the original
    % on the left side
    [X_l,Y_r,~] = align_nonrigid(data_l,data_r_mirror,"rigid");

    % Same method to have a plane of symetry but between on side and its
    % mirror image after alignement (better fit)
    [n_r,d_r,~,~]= find_plane_basic(Y_r,X_r,1);
    [n_l,d_l,~,~]= find_plane_basic(Y_l,X_l,1);

    % Norms of normal vectors
    norm_n_r = norm(n_r);
    norm_n_l= norm(n_l);
    % Standardised plans
    Plan_r = [n_r;d_r] / norm_n_r;
    Plan_l = [n_l;d_l] / norm_n_l;
    % Find the angular bisector plane, which is the average of the two planes found
    plane_final = Plan_r+Plan_l;

    % Construct the new coordinate system with the new plane and two
    % caractéristics points
    [~,Imin_x] = min(P_r(:,1));
    [~,Imax_z] = max(P_r(:,3));
    % We have to choose two points on the plane, the projection of
    % two extreme point
    [p1,~] = projection_distance(P_r(Imin_x,:), plane_final);
    [p2,~] = projection_distance(P_r(Imax_z,:), plane_final);
    n_final = [plane_final(1),plane_final(2),plane_final(3)];

    % Generate new coordinate system
    a1 = p2-p1 ; a1 = a1/norm(a1);
    a2 = cross(a1,n_final); a2=a2/norm(a2);
    a3 = cross(a1,a2); a3 = a3/norm(a3);
    % In order to have the pelvis in the right direction once the coordinate system changed
    if a3(1)<0
        a3=-a3;
    end
    system = [p1 a3 a1];

    % Generate mirror of each semi-pelvis along the final plane
    data_l_mirror = mirror(data_l,plane_final);
    data_r_mirror = mirror(data_r,plane_final);

    % Align the mirror image of the left-side semi-pelvis with the original
    % on the right side : we keep the Transform structure
    [~,~,Transform_r] = align_nonrigid(data_r,data_l_mirror,"rigid");
    % Align the mirror image of the right-side semi-pelvis with the original
    % on the left side : we keep the Transform structure
    [~,~,Transform_l] = align_nonrigid(data_l,data_r_mirror,"rigid");

end
```

Appendix B : function deviation.m

```
%% Deviation
% Gives the percentage of points below a deviation threshold as well as
% the mean distance (RMS) and standard deviation of this deviation
% To perform this analysis, for each point on one of the objects,
% we look for the triangle formed by the nearest neighbours of the point of interest
% on the mesh of the other object, and then calculate the deviation between
% the point of interest and its projection on this triangle.

% Input :
% P  : matrice nx3 containing a set of points which are the nodes of
% one of the two hemi-pelvis
% P_mirror : matrice nx3 containing a set of points which are the nodes of
% the mirror of P (after or before the alignement step)
% ConnectivityList : matrice nx3 with the trio of indexes of the nodes of P
% which form the triangles of its mesh
% d : threshold of deviation
% v : number of neighbours on the other surface taken into account in the search for the nearest triangle
% k : step of nodes taken by the algortithm

% Output :
% distance : deviation calculated between nodes of P_mirror and their
% projection on the surface of P
% RMS : root mean square of the absolute deviation betwwen the surfaces of P_mirror
% and P
% s : standard deviation of the deviation
% rate : percentage of P_mirror nodes taken into account by the algorithm
% C_distance : vector of 0,1 and 2 where
    % 0 : The node is not taken into account because we don't find any
    % triangle formed by nodes on the other mesh close to the node of interest
    % 1 : The deviation for that node is below the threshold d
    % 2 : The deviation for that node is above the threshold d
% out : Vector of point with deviation above 5 mm
```

```
function [distance, RMS, s, rate, C_distance, out]=deviation(P_mirror, P, ConnectivityList, d, v, k)
    % We sort the connectiviy list in order to have a faster lecture of
    % this matrice
    ConnectivityList = sort(ConnectivityList, 2);
    % Init new matrices
    distance = [];
    projection = [];
    out = [];
    C_distance = zeros(size(P_mirror, 1), 1);
    % Calcul deviation for each node of P_mirror
    % We can use k as step if we don't want to use all the nodes
    for i = 1:k:size(P_mirror,1)
        % Find the v nearest neightbors of the node i on the mesh of the
        % original pelvis by calculating the vector norm
        [~,idx] = mink(vecnorm(P_mirror(i, :)-P, 2, 2), v);
        % Generate all combinations of 3 indices from among those in the vector
        combinations = nchoosek(idx, 3);
        % Go through each combination and find the trio that form triangle in the mesh
        for j = 1:size(combinations, 1)
            comb = combinations(j, :);
            comb = sort(comb);
            triangle = ismember(ConnectivityList, comb, "rows");
            triangle(triangle==0) = [];
            % If the trio forms a triangle, we calculate
            % the distance between the node and its projection (the deviation)
            % on the plane formed by this triangle
            if ~isempty(triangle)
                [n,~,p] = affine_fit(P(comb, :));
                o = -dot(n,p);
                plane = [n',o];
                [proj,dist] = projection_distance(P_mirror(i,:), plane);
                distance = [distance, dist];
                projection = [projection; proj];
                % Classify this node according to this deviation
                if abs(dist)>5
                    out = [out; i];
                end
                if abs(dist)>d
                    C_distance(i) = 2;
                else
                    C_distance(i) = 1;
                end
                break % Stops the loop as soon as we have a triangle
            end
        end
    end
    % Calculate the rate of nodes below the treshold of deviation
    rate = (sum(abs(distance)<=d)/length(distance))*100;
    % Calculate the RMS (Root Mean Square) of the deviation
    N = length(distance);
    RMS = sqrt((1/N)*sum(abs(distance).^2));
    % Calculate the standard deviation of the deviation
    s = std(distance);
    % Show the percentage of node taken into account (just to have an idea
    % of the losses)
    take_into_account = 100*length(distance)/(i/k);
    disp(take_into_account)
end
```

Appendix C: Tables of data

Subject	1	2	3	4	5	6	7	8	9	10
Age	66	71	56	22	57	80	49	23	29	65
Sex	W	M	W	M	W	M	W	M	W	M
Deviation plan (%)	41,905	81,860	92,870	52,515	87,885	73,245	81,000	69,235	60,550	70,550
Deviation (%)	87,685	91,230	94,730	91,285	97,265	81,190	94,275	91,750	93,105	91,330
RMS plan (mm)	3,355	1,615	1,095	3,065	1,295	1,850	1,615	1,920	2,370	1,880
RMS (mm)	1,375	1,320	0,970	1,165	0,860	1,565	0,980	1,185	1,130	1,205
Difference translation (mm)	1,070	1,870	0,410	6,980	0,710	1,630	0,700	1,870	1,650	1,390
Left_sphere (mm)	23,127	29,045	23,270	25,381	22,527	29,326	23,854	26,104	24,184	26,723
Right_sphere (mm)	23,831	29,627	23,315	25,544	22,238	29,183	24,775	26,424	23,581	26,778
Mean_sphere (mm)	23,479	29,336	23,292	25,462	22,383	29,254	24,314	26,264	23,883	26,751
Diff_sphere (%)	0,704	0,581	0,045	0,163	0,289	0,143	0,921	0,320	0,603	0,055
Left_volume ($x10^4$ mm^3)	33,043	47,265	26,225	40,911	26,643	44,784	26,710	29,575	34,608	40,224
Right_volume ($x10^4$ mm^3)	32,333	48,478	25,728	40,933	26,941	44,547	26,785	29,997	35,023	40,024
Mean_volume ($x10^4$ mm^3)	32,688	47,871	25,976	40,922	26,792	44,666	26,748	29,786	34,815	40,124
Diff_volume (%)	2,148	2,504	1,895	0,052	1,106	0,529	0,279	1,408	1,185	0,496
Left_surface ($x10^4$ mm^2)	6,014	7,391	5,348	6,391	4,984	7,360	5,141	5,760	5,395	7,072
Right_surface ($x10^4$ mm2)	5,941	7,457	5,288	6,334	5,035	7,385	5,211	5,764	5,462	7,064
Mean_surface ($x10^4$ mm2)	5,978	7,424	5,318	6,363	5,009	7,372	5,176	5,762	5,428	7,068
Diff _surface (%)	1,220	0,889	1,111	0,898	1,019	0,343	1,351	0,083	1,218	0,106

Subject	11	12	13	14	15	16	17	18	19	20
Age	51	68	84	38	64	84	65	76	45	32
Sex	W	M	M	W	M	M	M	M	M	W
Deviation plan (%)	34,115	73,975	79,630	40,365	71,935	65,340	64,170	81,810	85,085	79,810
Deviation (%)	88,700	86,620	94,935	89,535	88,455	90,560	88,120	93,200	93,150	96,050
RMS plan (mm)	4,215	2,015	1,570	4,070	1,900	2,045	2,125	1,470	1,385	1,550
RMS (mm)	1,290	1,360	1,010	1,255	1,290	1,290	1,290	1,050	1,050	0,915
Difference translation (mm)	1,450	1,830	1,030	1,440	1,670	1,100	5,710	1,020	0,570	0,970
Left_sphere (mm)	23,609	24,623	25,349	22,818	24,828	27,041	23,409	26,015	26,732	24,924
Right_sphere (mm)	23,557	25,360	25,385	23,176	23,985	27,098	23,487	26,038	27,706	25,268
Mean_sphere (mm)	23,583	24,991	25,367	22,997	24,406	27,069	23,448	26,027	27,219	25,096
Diff_sphere (%)	0,053	0,737	0,036	0,358	0,843	0,057	0,079	0,023	0,974	0,345
Left_volume ($x10^4$ mm^3)	26,052	34,778	34,870	29,936	36,584	31,696	25,428	38,359	40,053	30,809
Right_volume ($x10^4$ mm^3)	26,300	35,242	35,353	29,039	34,821	32,930	26,511	38,813	39,354	30,433
Mean_volume ($x10^4$ mm^3)	26,176	35,010	35,111	29,487	35,702	32,313	25,969	38,586	39,703	30,621
Diff_volume (%)	0,943	1,316	1,365	2,995	4,819	3,748	4,085	1,169	1,745	1,219
Left_surface ($x10^4$ mm^2)	5,248	6,098	6,258	5,584	6,735	6,068	4,922	6,820	6,568	5,305
Right_surface ($x10^4$ mm^2)	5,286	6,090	6,303	5,453	6,509	6,140	5,073	6,828	6,512	5,247
Mean_surface ($x10^4$ mm^2)	5,267	6,094	6,280	5,519	6,622	6,104	4,998	6,824	6,540	5,276
Diff _surface (%)	0,723	0,130	0,722	2,334	3,366	1,160	2,973	0,120	0,851	1,103

Subject	21	22	23	24	25	26	27	28	Mean	Standard Deviation
Age	24	83	39	83	58	29	63	66	56,071	20,149
Sex	M	W	W	W	W	M	W	W		
Deviation plan (%)	42,750	64,450	51,090	71,460	39,715	87,970	60,635	61,385	66,689	16,472
Deviation (%)	97,230	91,675	94,040	90,345	86,375	95,300	88,650	94,860	91,487	3,707
RMS plan (mm)	2,520	2,035	2,615	1,775	3,685	1,285	2,470	2,110	2,175	0,827
RMS (mm)	0,825	1,175	0,950	1,205	1,410	0,990	1,280	1,010	1,157	0,183
Difference translation (mm)	1,560	1,600	1,830	1,190	2,520	0,540	1,550	1,300	1,684	1,413
Left_sphere (mm)	27,980	22,869	22,405	24,242	22,771	26,104	22,786	23,519	24,842	1,972
Right_sphere (mm)	27,773	22,779	22,953	24,704	22,629	26,424	22,969	24,070	25,023	2,016
Mean_sphere (mm)	27,876	22,824	22,679	24,473	22,700	26,264	22,878	23,794	24,933	1,983
Diff_sphere (%)	0,207	0,090	0,548	0,462	0,142	0,320	0,183	0,551	0,351	0,293
Left_volume ($x10^4$ mm^3)	38,841	25,565	20,751	33,953	23,324	31,720	29,099	25,627	32,408	6,700
Right_volume ($x10^4$ mm^3)	37,275	24,891	20,969	35,025	23,452	32,099	29,060	26,333	32,453	6,669
Mean_volume ($x10^4$ mm^3)	38,058	25,228	20,860	34,489	23,388	31,910	29,080	25,980	32,431	6,674
Diff_volume (%)	4,031	2,638	1,038	3,061	0,547	1,182	0,132	2,680	1,797	1,293
Left_surface ($x10^4$ mm^2)	6,336	4,925	4,760	6,200	5,043	6,037	5,402	5,147	5,868	0,771
Right_surface ($x10^4$ mm^2)	6,222	4,877	4,789	6,282	5,035	6,049	5,364	5,224	5,865	0,759
Mean_surface ($x10^4$ mm^2)	6,279	4,901	4,775	6,241	5,039	6,043	5,383	5,185	5,867	0,764
Diff _surface (%)	1,788	0,973	0,608	1,294	0,153	0,197	0,705	1,468	1,032	0,813

BIBLIOGRAPHY

1. Merema, B. J. *et al.* The design, production and clinical application of 3D patient-specific implants with drilling guides for acetabular surgery. *Injury* **48**, 2540–2547 (2017).
2. The Pelvic Girdle - Structure - Function - Assessment - TeachMeAnatomy. https://teachmeanatomy.info/pelvis/bones/pelvic-girdle/.
3. The Hip Bone - Ilium - Ischium - Pubis - TeachMeAnatomy. https://teachmeanatomy.info/pelvis/bones/hip-bone/.
4. Pr MERTENS. Pelvis osseux. *SlideShare* https://fr.slideshare.net/latifahanachi/04-fractures-du-cotyle-1 (2014).
5. Lecturio - Drawing Sagittal, coronal and transverse plane - English labels | AnatomyTOOL. https://anatomytool.org/content/lecturio-drawing-sagittal-coronal-and-transverse-plane-english-labels.
6. Albrektsson, M., Möller, M., Wolf, O., Wennergren, D. & Sundfeldt, M. Acetabular fractures: Epidemiology and mortality based on 2,132 fractures from the Swedish Fracture Register. *Bone & joint open* **4**, 652–658 (2023).
7. Letournel, E. Acetabulum fractures: classification and management. *Clin Orthop Relat Res* 81–106 (1980).
8. Stahel, P. & Hammerberg, E. History of pelvic fracture management: A review. *World Journal of Emergency Surgery* **11**, (2016).
9. Alton, T. B. & Gee, A. O. Classifications in Brief: Letournel Classification for Acetabular Fractures. *Clinical Orthopaedics and Related Research®* **472**, 35 (2014).
10. Judet, R., Judet, J. & Letournel, E. FRACTURES OF THE ACETABULUM: CLASSIFICATION AND SURGICAL APPROACHES FOR OPEN REDUCTION. PRELIMINARY REPORT. *J Bone Joint Surg Am* **46**, 1615–1646 (1964).

11. Matta, J. M. Fractures of the acetabulum: accuracy of reduction and clinical results in patients managed operatively within three weeks after the injury. *J Bone Joint Surg Am* **78**, 1632–1645 (1996).

12. Dakin, G. J., Eberhardt, A. W., Alonso, J. E., Stannard, J. P. & Mann, K. A. Acetabular fracture patterns: associations with motor vehicle crash information. *J Trauma* **47**, 1063–1071 (1999).

13. Ohashi, K., El-Khoury, G. Y., Abu-Zahra, K. W. & Berbaum, K. S. Interobserver agreement for Letournel acetabular fracture classification with multidetector CT: are standard Judet radiographs necessary? *Radiology* **241**, 386–391 (2006).

14. Jindal, K., Aggarwal, S., Kumar, P. & Kumar, V. Complications in patients of acetabular fractures and the factors affecting the quality of reduction in surgically treated cases. *Journal of Clinical Orthopaedics and Trauma* **10**, 884–889 (2019).

15. Yücens, M., Aydemir, N. & Demirkan, A. ASSESSMENT OF INTEROBSERVER RELIABILITY FOR THE LETOURNEL AND JUDET CLASSIFICATION. *Acta Ortopédica Brasileira* **32**, (2024).

16. Bucholz, R. W. The pathological anatomy of Malgaigne fracture-dislocations of the pelvis. *J Bone Joint Surg Am* **63**, 400–404 (1981).

17. Young, J. W. R., Burgess, A. R., Brumback, R. J. & Poka, A. Lateral compression fractures of the pelvis: The importance of plain radiographs in the diagnosis and surgical management. *SKELETAL RADIOL.* **15**, 103–109 (1986).

18. Tile, M. Acute Pelvic Fractures: II. Principles of Management. *JAAOS - Journal of the American Academy of Orthopaedic Surgeons* **4**, 152 (1996).

19. Giannoudis, P. V., Grotz, M. R. W., Papakostidis, C. & Dinopoulos, H. Operative treatment of displaced fractures of the acetabulum. A meta-analysis. *J Bone Joint Surg Br* **87**, 2–9 (2005).

20. Dias, M. V. F. *et al.* EPIDEMIOLOGY OF ACETABULUM FRACTURES TREATED AT THE INSTITUTO NACIONAL DE TRAUMATOLOGIA E ORTOPEDIA (INTO). *Rev Bras Ortop* **45**, 474–477 (2010).

21. A, K., Na, S., Sa, K. & Ad, C. Operative management of acetabular fractures. A review of 73 fractures. *Injury* **36**, (2005).

22. Heeg, M., Klasen, H. J. & Visser, J. D. Operative treatment for acetabular fractures. *J Bone Joint Surg Br* **72**, 383–386 (1990).

23. Brueton, R. N. A review of 40 acetabular fractures: the importance of early surgery. *Injury* **24**, 171–174 (1993).

24. Boudissa, M., Oliveri, H., Chabanas, M. & Tonetti, J. Computer-assisted surgery in acetabular fractures: Virtual reduction of acetabular fracture using the first patient-specific biomechanical model simulator. *Orthop Traumatol Surg Res* **104**, 359–362 (2018).

25. Tissingh, E. K., Johnson, A., Queally, J. M. & Carrothers, A. D. Fix and replace: An emerging paradigm for treating acetabular fractures in older patients. *World Journal of Orthopedics* **8**, 218 (2017).

26. Rickman, M., Mbbs, J. Y., Mbbs, A. T., Pearce, R. & Frca, M. H. Managing Acetabular Fractures in the Elderly With Fixation and Primary Arthroplasty. *Clinical Orthopaedics and Related Research* **472**, (2014).

27. Kim, J. W. *et al.* Acetabular fractures in elderly patients: a comparative study of low-energy versus high-energy injuries. *International Orthopaedics (SICOT)* **39**, 1175–1179 (2015).

28. Heimke, I. M., Scarcella, N. R., Simske, N. M., Furdock, R. & Vallier, H. A. Surgical Versus Nonsurgical Management of Acetabular Fractures With Associated Patterns in Elderly Patients: Factors Affecting Outcomes. *J Am Acad Orthop Surg Glob Res Rev* **6**, e22.00014 (2022).

29. World Health Organization, Musculoskeletal Trauma. http://who.mgsolutions-it.com/MusculoskeletalTrauma.aspx.

30. Rommens, P. M. *et al.* Open reduction and internal fixation of acetabular fractures in patients of old age. *International Orthopaedics (SICOT)* **44**, 2123–2130 (2020).

31. Kumar, R., Sharma, D., Bhushan, B., Lal, M. & Kashyap, S. Evaluation of Functional Outcome and Complications after Open Reduction and Internal Fixation of Acetabulum Fractures. *IAR Journal of Medical Sciences* **3**, 100–105 (2022).

32. Ali, E. Acetabular Fractures - A Review of their Management. *Journal of Trauma & Treatment* **04**, (2015).

33. Gautam, D., Gupta, S. & Malhotra, R. Total hip arthroplasty in acetabular fractures. *J Clin Orthop Trauma* **11**, 1090–1098 (2020).

34. Paprosky, W. G., Perona, P. G. & Lawrence, J. M. Acetabular defect classification and surgical reconstruction in revision arthroplasty. A 6-year follow-up evaluation. *J Arthroplasty* **9**, 33–44 (1994).

35. Shon, W. Y., Santhanam, S. S. & Choi, J. W. Acetabular Reconstruction in Total Hip Arthroplasty. *Hip Pelvis* **28**, 1–14 (2016).

36. Revision Total Hip Replacement - OrthoInfo - AAOS. https://www.orthoinfo.org/en/treatment/revision-total-hip-replacement/.

37. Bozzio, A. E., Wydra, F. B., Mitchell, J. J., Ackerson, R. M. & Mauffrey, C. Percutaneous Fixation of Anterior and Posterior Column Acetabular Fractures. *Orthopedics* **37**, 675–678 (2014).

38. Gay, S. B. *et al.* Percutaneous screw fixation of acetabular fractures with CT guidance: preliminary results of a new technique. *AJR Am J Roentgenol* **158**, 819–822 (1992).

39. Einhorn, S. *et al.* Comparison of Percutaneous Screw Fixation to Open Reduction and Internal Fixation in Acetabular Fractures: A Matched Pair Study Regarding the Short-Term Rate

of Conversion to Total Hip Arthroplasty and Functional Outcomes. *Journal of Clinical Medicine* **12**, 1163 (2023).

40. Madhu, R. *et al.* Outcome of surgery for reconstruction of fractures of the acetabulum. The time dependent effect of delay. *J Bone Joint Surg Br* **88**, 1197–1203 (2006).

41. Ochs, B. G. *et al.* Changes in the treatment of acetabular fractures over 15 years: Analysis of 1266 cases treated by the German Pelvic Multicentre Study Group (DAO/DGU). *Injury* **41**, 839–851 (2010).

42. Mears, D. C. Pelvic and Acetabular Fractures. in *Cannulated Screw Fixation: Principles and Operative Techniques* (eds. Asnis, S. E. & Kyle, R. F.) 97–145 (Springer, New York, NY, 1996). doi:10.1007/978-1-4612-2326-9_7.

43. Dl, H. & Gj, S. Management of complex acetabular fractures through single nonextensile exposures. *Clinical orthopaedics and related research* (1994).

44. Gupta, R. K. *et al.* Results of operative treatment of acetabular fractures from the Third World—how local factors affect the outcome. *Int Orthop* **33**, 347–352 (2009).

45. Lundin, N., Berg, H. E. & Enocson, A. Complications after surgical treatment of acetabular fractures: a 5-year follow-up of 229 patients. *Eur J Orthop Surg Traumatol* **33**, 1245–1253 (2023).

46. Operative management of acetabular fractures in Oxford - PubMed. https://pubmed.ncbi.nlm.nih.gov/11524093/.

47. Maini, L. *et al.* Evaluation of accuracy of virtual surgical planning for patient-specific pre-contoured plate in acetabular fracture fixation. *Arch Orthop Trauma Surg* **138**, 495–504 (2018).

48. Meesters, A. *et al.* Introduction of a three-dimensional computed tomography measurement method for acetabular fractures. *PLOS ONE* **14**, e0218612 (2019).

49. Weidert, S. *et al.* 3D printing method for next-day acetabular fracture surgery using a surface filtering pipeline: feasibility and 1-year clinical results. *Int J Comput Assist Radiol Surg* **15**, 565–575 (2020).

50. Upex, P., Jouffroy, P. & Riouallon, G. Application de l'impression 3D au traitement d'une fracture des deux colonnes de l'acétabulum : intérêt pour le prémoulage des plaques sur le bassin sain en miroir. *Revue de Chirurgie Orthopédique et Traumatologique* **103**, 227–230 (2017).

51. Chana Rodríguez, F., Pérez Mañanes, R., Narbona Cárceles, F. J. & Gil Martínez, P. 3D printing utility for surgical treatment of acetabular fractures. *Rev Esp Cir Ortop Traumatol (Engl Ed)* **62**, 231–239 (2018).

52. Boulay, C. *et al.* Three-dimensional study of pelvic asymmetry on anatomical specimens and its clinical perspectives. *J Anat* **208**, 21–33 (2006).

53. Ead, M. S., Duke, K. K., Jaremko, J. L. & Westover, L. Investigation of pelvic symmetry using CAD software. *Med Biol Eng Comput* **58**, 75–82 (2020).

54. Zheng, Q. *et al.* Investigation of pelvic symmetry: A systematic analysis using computer aided design software. *Health Care Science* **2**, 36–44 (2023).

55. CT (Computed Tomography) Scan: What It Detects. *Cleveland Clinic* https://my.clevelandclinic.org/health/diagnostics/4808-ct-computed-tomography-scan.

56. Materialise aMace | Personalized Acetabular Implants. https://www.materialise.com/en/healthcare/amace-acetabular-hip-implant.

57. Eltes, P. *et al.* Geometrical accuracy evaluation of an affordable 3D printing technology for spine physical models. *Journal of Clinical Neuroscience* **72**, (2020).

58. Myronenko, A. & Song, X. Point Set Registration: Coherent Point Drift. *IEEE Transactions on Pattern Analysis and Machine Intelligence* **32**, 2262–2275 (2010).

59. Van den Broeck, J., Vereecke, E., Wirix-Speetjens, R. & Vander Sloten, J. Segmentation accuracy of long bones. *Medical Engineering & Physics* **36**, 949–953 (2014).